Chapter 4. Reconstructed Aerosol Light Extinction Coefficients

Light extinction occurs in the atmosphere when incident light is attenuated by the scattering and absorption of light from particles and gases in the layer through which it travels. The light extinction coefficient (b_{ext}) is the fractional loss of intensity per unit path length. The Beer-Lambert law describes the intensity (F) of an incident flux (F_o) through a layer of thickness (z) as

$$\frac{F}{F_o} = \exp(-b_{ext} z) . \quad (4.1)$$

The extinction coefficient can be written as the sum of scattering and absorption by particles (b_{sp} and b_{ap}, respectively) and gases (b_{sg} and b_{ag}, respectively) and has units of inverse length:

$$b_{ext} = b_{sp} + b_{ap} + b_{sg} + b_{ag}. \quad (4.2)$$

Absorption of light by gases is a well-understood phenomenon and straightforward to estimate. Visible light absorption by gases in the atmosphere is dominated by nitrogen dioxide (NO_2) and can be estimated by multiplying NO_2 concentrations by an absorption efficiency (Pitchford et al., 2007). Rayleigh scattering theory describes scattering of light by molecules (b_{sg}) and depends on the density of the atmosphere. The highest Rayleigh scattering values occur at sea level (~12 Mm^{-1} at 550 nm), compared to the lowest levels at high elevations (8 Mm^{-1} at 550 nm at ~3.0 km). Rayleigh scattering can vary due to temperature and pressure variations; it can be accurately determined if elevation and meteorological conditions are known.

Light extinction by particles is more complicated and depends strongly on particle size, composition, and hygroscopic properties. All particles scatter light and, if their size and refractive index are known, light scattering coefficients can be computed using Mie theory, assuming spherical particles. Light absorption by particles in the visible wavelengths is due to light absorbing carbon as well as some crustal mineral species. Because all of the required information necessary for performing Mie calculations is typically unknown (size distribution and concurrent aerosol composition measurements are time intensive and costly), the IMPROVE algorithm was developed to estimate aerosol light extinction coefficients based on assumed size distributions and composition measurements (Malm et al., 1994).

4.1 IMPROVE AEROSOL LIGHT EXTINCTION COEFFICIENT ALGORITHM

Light extinction coefficients can be computed for an external mixture of aerosols by assuming a linear combination of species mass concentrations:

$$b_{ext} = \sum_j \alpha_j M_j . \quad (4.3)$$

The species (j) mass concentration is given by M_j ($\mu g\ m^{-3}$), and the dry speices mass extinction efficiency is given by α_j ($m^2\ g^{-1}$) (Hand and Malm, 2007). Equation (4.3) holds for an internally mixed aerosol where the chemical species are mixed in fixed proportions to each other,

the index of refraction is not a function of composition or size, and the aerosol density is independent of volume (Malm and Kreidenweis, 1997).

For species that absorb water, the linear relationship between light extinction coefficients and mass shown in equation (4.3) will not hold because of the nonlinear behavior of particle growth and b_{ext} with increased relative humidity (RH). To account for this effect, the extinction efficiencies are multiplied by a humidification factor ($f(RH) = b_{sp,RH}/b_{sp,dry}$) that is the ratio of humidified (b_{sp_RH}) to dry (b_{sp_dry}) light scattering coefficients. Humidification factors are computed by assuming a size distribution and using composition-dependent growth factors.

The original IMPROVE equation has been used extensively to reconstruct b_{ext}, using measured aerosol composition (e.g., Malm et al., 1994; Lowenthal and Kumar, 2003; Malm et al., 2005; Malm and Hand, 2007; Prenni et al., 2019), and was adopted by the Environmental Protection Agency (EPA) as a metric for tracking progress in reducing haze levels under the 1999 Regional Haze Rule (RHR) (Pitchford et al., 2007). In 2005 a review was initiated by the IMPROVE steering committee to investigate possible biases in reconstructed light extinction coefficients as computed by the original algorithm (Hand and Malm, 2006; Malm and Hand, 2007). The review resulted in the development of the second IMPROVE algorithm that is now being used by most states in their state implementation plans (Pitchford et al., 2007).

Modifications made for the second IMPROVE algorithm included the addition of a sea salt (SS) term with associated hygroscopic growth; a change in the organic mass (OM) to organic carbon (OC) ratio (OM/OC) from 1.4 to 1.8 to calculate particulate organic mass from organic carbon (POM = (OM/OC)×OC); the use of site-specific Rayleigh scattering values rather than a constant 10 Mm^{-1}; and a split-component mass extinction efficiency algorithm for ammonium sulfate (AS), ammonium nitrate (AN), and POM to approximate a bimodal size distribution. The second IMPROVE equation also included light absorption for NO_2 (Pitchford et al., 2007) for locations with these measurements; this term is not included in the analysis here.

Recent examinations of biases between gravimetric and reconstructed fine mass and measured and reconstructed scattering have identified issues with the reconstructed mass and extinction algorithms, resulting in underestimations of reconstructed mass and extinction over time (Hand et al., 2019; Prenni et al., 2019). As discussed in Chapter 2, biases associated with the OM/OC ratio and underestimates of fine dust (FD) were identified as major contributors to the mass bias and were accounted for by applying monthly values of OM/OC and increasing FD by 15%. Biases in measured and reconstructed scattering were associated with the split-component mass extinction efficiency algorithm used to approximate bimodal size distributions for AS, AN, and POM. A potential correction to the reconstructed extinction algorithm was proposed by Prenni et al. (2019) but has not been finalized.

Given the changes to the reconstructed mass algorithm and issues related to the split-component extinction algorithm, the approach for calculating reconstructed extinction in this report is a modified version of the original IMPROVE algorithm (single size mode model), with the addition of SS and site-specific Rayleigh scattering. In addition, POM was calculated with monthly varying OM/OC ratios as described in Chapter 2, and FD was increased by 15%. The algorithm for calculating ambient total b_{ext} (b_{ext_tot}) is presented in equation (4.4):

$$b_{ext\_tot} = 3\times f(RH)\times[AS] + 3\times f(RH)\times[AN] + 4\times[POM] + 10\times[EC] + 1\times[FD] + 1.7\times f(RH)_{ss}\times[SS] + 0.6\times[CM] + \text{site-specific Rayleigh scattering} \quad (4.4)$$

EC is elemental carbon and CM is coarse mass. The units of b_{ext_tot} and Rayleigh scattering are in inverse megameters (Mm^{-1}). Mass concentrations of aerosol species are in units of $\mu g\ m^{-3}$, and mass extinction efficiencies have units of $m^2\ g^{-1}$. Dry mass extinction efficiencies (numerals multiplying each term in equation 4.4) were rounded to one significant digit to represent the degree of uncertainty associated with these values. Values of 3 $m^2\ g^{-1}$ were used for both AS and AN, 4 $m^2\ g^{-1}$ for POM, 10 $m^2\ g^{-1}$ for EC, 1 $m^2\ g^{-1}$ for FD, 1.7 $m^2\ g^{-1}$ for SS, and 0.6 $m^2\ g^{-1}$ for CM. These values correspond to a wavelength of 550 nm (Hand and Malm, 2007). Extinction coefficients for individual species correspond to their individual terms in equation (4.4).

The f(RH) values applied in equation (4.4) were computed using the algorithm outlined in the Regional Haze Rule Guidelines for Tracking Progress (EPA, 2003) and were the same values applied in previous IMPROVE reports. The f(RH) curve was calculated with Mie theory, assuming a lognormal AS mass size distribution with a geometric mass mean diameter of 0.3 µm and a geometric standard deviation of 2.0 and interpolated between the deliquescence and efflorescence points. This f(RH) was applied to both AS and AN (see Figure 4.1a). The $f(RH)_{ss}$ curve applied to SS was computed assuming a SS geometric mass mean diameter of 2.5 µm and a geometric standard deviation of 2 and is shown in Figure 4.1b (Pitchford et al., 2007). Below the deliquescence point (RH = 47%) the $f(RH)_{SS}$ is set to 1. POM was assumed to be nonhygroscopic. Humidification factors are unitless.

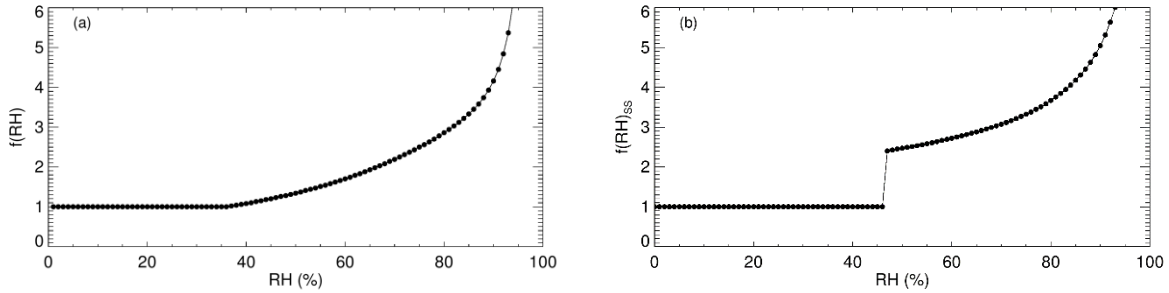

Figure 4.1. (a) Humidification factors (f(RH)) as a function of relative humidity (RH, %) for AS. A lognormal mass size distribution with a geometric mass mean diameter of 0.3 µm and a geometric standard deviation of 2.0 was assumed. (b) $f(RH)_{SS}$ for SS with an assumed lognormal mass size distribution with a geometric mass mean diameter of 2.5 µm and a geometric standard deviation of 2.0. A wavelength of 550 nm was used.

Monthly and site-specific f(RH) curves were generated based on monthly climatological mean RH values. These monthly RH values eliminate the effects of interannual variations in RH while maintaining typical regional and seasonal humidity patterns around the United States. The EPA produced recommended monthly f(RH) values for each Class I area, based on analysis of a 10-year record (1988–1997) of hourly RH data from 292 National Weather Service stations across the 50 states and the District of Columbia, as well as from 29 IMPROVE and IMPROVE-protocol monitoring sites, 48 Clean Air Status and Trends Network (CASTNet) sites, and 13 additional sites administered by the National Park Service. Values of f(RH) for other IMPROVE sites (non-Class I area sites) were generated using an interpolation scheme with an inverse distance weighting technique (EPA, 2001). The daily ambient AS, AN, and SS extinction

coefficients for each site were calculated using this lookup table. Values of f(RH) vary significantly depending on time of year and site location. For example, the f(RH) value at Great Basin National Park (NP), Nevada (GRBA1), in August is assumed to be 1.23, compared to 4.16 in at Redwood NP, California (REDW1). Estimates of f(RH) for Chemical Speciation Network (CSN) sites were determined similarly to non-Class I area IMPROVE sites by using an interpolation scheme. Values of f(RH) and site-specific Rayleigh scattering values used in this report are provided in Appendix 4.1 and 4.2 (IMPROVE and the CSN, respectively).

Visual range and extinction measurements are nonlinear with respect to human perception of visual scene changes caused by haze. The deciview (dv) haze index was derived with a number of assumptions such that uniform changes in haze correspond to approximately uniform incremental changes in visual perception (Pitchford and Malm, 1994). Deciview is calculated from reconstructed b_{ext_tot}, using equation (4.5):

$$dv = 10 \times \ln(b_{ext\_tot}/10) \quad (4.5)$$

In the original IMPROVE equation, dv = 0 for pristine (Rayleigh scattering) conditions (elevation ~1.8 km) for elevations where Rayleigh scattering = 10 Mm^{-1}. For different values of site-specific Rayleigh scattering, as specified in equation (4.4), it is possible to have a negative dv for pristine conditions (b_{ext_tot} <10 Mm^{-1}).

Daily b_{ext} values were computed using equation (4.4) for AS, AN, POM, EC, FD, SS, CM, reconstructed aerosol b_{ext} (b_{ext_aer} = sum of speciated b_{ext}), b_{ext_tot} ($b_{ext\_tot} = b_{ext\_aer}$ + site-specific Rayleigh scattering), and dv for IMPROVE and CSN sites. Monthly, seasonal, and annual means were computed following the methods and completeness criteria outlined in Chapter 2. Spatial patterns of 2016–2019 annual mean speciated b_{ext} are presented. Differences between patterns in mass and b_{ext} are likely due to hygroscopic effects for species that uptake water. For nonhygroscopic species, b_{ext} values are scaled mass concentrations. Fractional contributions of speciated b_{ext} to b_{ext_aer} are also presented. The top number in the scale of each contour map corresponds to the maximum b_{ext} for all sites, although the contours themselves were created with the highest level set to the 95th percentile in b_{ext}. Interpolated data are provided only to reflect general spatial patterns, not for strict interpretation.

Recall from Chapter 2 that CM is not available at CSN sites. For CSN, an estimate of urban CM b_{ext} (b_{ext_CM}) was made by interpolating 2016–2019 monthly averaged EPA CM concentrations to CSN site locations. These interpolated monthly mean values were used to calculate daily estimates of b_{ext_aer}, b_{ext_tot}, and dv at CSN sites. Comparisons of 2016–2019 monthly mean CM concentrations at collocated IMPROVE (measured) and CSN (interpolated) sites are shown in Figure 4.2 for Birmingham, Alabama (BIRM1), Fresno, California (FRES1), Phoenix, Arizona (PHOE1), and Puget Sound, Washington (PUSO1). Concentrations were highly correlated (r = 0.99); however, monthly mean IMPROVE CM was higher than collocated interpolated CSN CM, with a 12% bias. For context, recall that biases between IMPROVE and CSN FD and SS were greater (20% and 81%, respectively), with higher IMPROVE values (see Chapter 1). CM was not interpolated at sites in Alaska or Hawaii, so b_{ext_aer}, b_{ext_tot}, dv, and fractional contributions of b_{ext_CM} to b_{ext_aer} were not calculated at those sites.

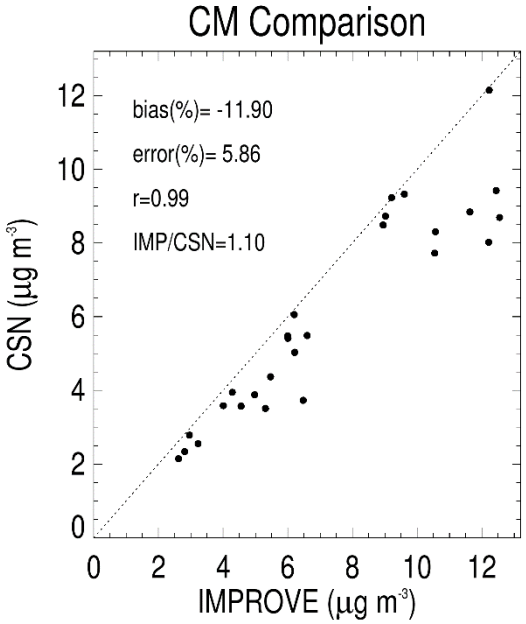

Figure 4.2. Comparisons of 2016–2019 monthly mean coarse mass concentrations (CM, µg m^{-3}) for four collocated IMPROVE (measured) and CSN (interpolated) sites. CSN CM concentrations were spatially interpolated from EPA Federal Reference Method (FRM) sites.

4.2 SPATIAL PATTERNS IN ANNUAL MEAN AEROSOL LIGHT EXTINCTION COEFFICIENTS

4.2.1 $PM_{2.5}$ Ammonium Sulfate Light Extinction Coefficients

The 2016–2019 IMPROVE rural annual mean light extinction coefficients corresponding to AS (b_{ext_AS}) ranged from 1.67 Mm^{-1} in Sawtooth National Forest (NF), Idaho (SAWT1), to 19.52 Mm^{-1} in Breton Island, Louisiana (BRIS1) (Figure 4.2.1a). Annual mean b_{ext_AS} was higher at sites in the eastern United States relative to the western United States. A similar pattern was observed for annual mean AS mass concentrations in Chapter 2. The highest values of annual mean b_{ext_AS} occurred at sites along the Ohio River valley and the Gulf Coast regions in Louisiana and Florida (>15 Mm^{-1}). At sites in the Intermountain West, b_{ext_AS} was typically less than 5 Mm^{-1}. Although AS annual mean mass concentrations increased along the southern coast of California, this increase was not as obvious for b_{ext_AS}, perhaps due in part to lower relative humidity and hygroscopic effects in that region relative to regions in the East.

Similar spatial patterns of b_{ext_AS} were observed with the addition of CSN sites (Figure 4.2.1b), with higher values at sites along the Ohio River valley and Gulf region, with a strong East-West gradient and low values in the western United States. The maximum annual mean b_{ext_AS} for the CSN network occurred in Liberty, Pennsylvania (29.36 Mm^{-1}, 420030064), compared to the lowest b_{ext_AS} in Reno, Nevada (2.37 Mm^{-1}, 320310016). The similarity in the spatial patterns and magnitudes of b_{ext_AS} for the IMPROVE and CSN sites suggest sources and meteorological conditions that contribute to high b_{ext_AS} on regional scales.

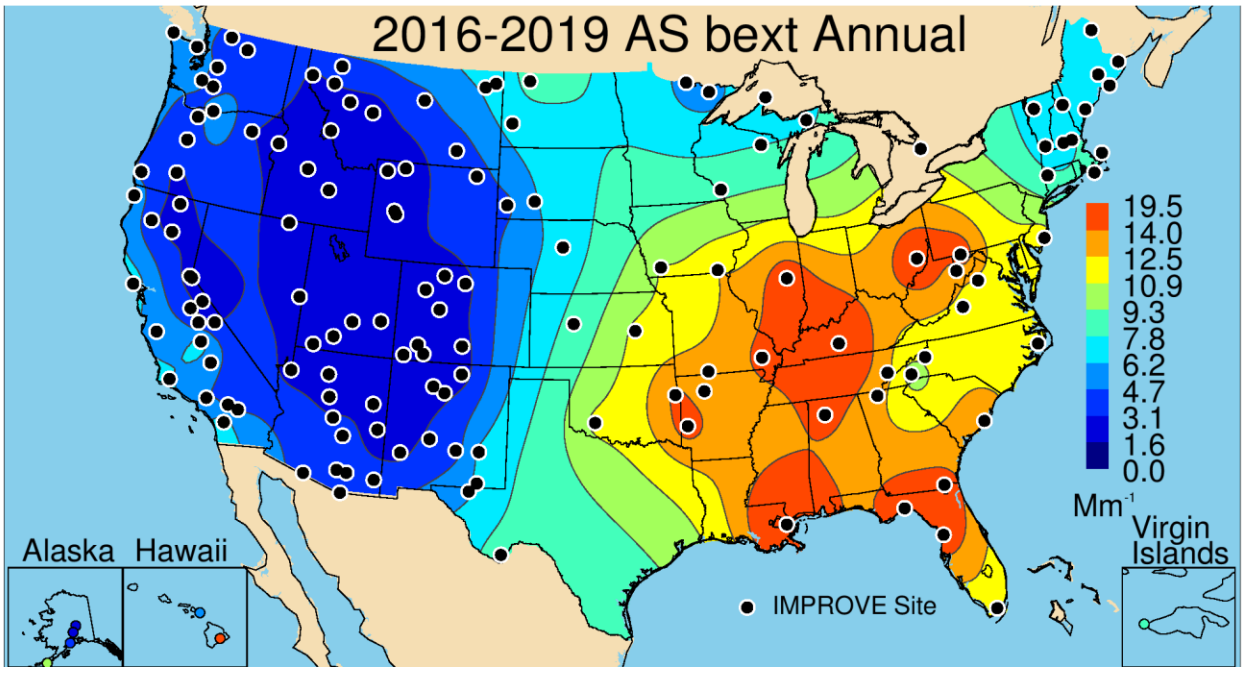

Figure 4.2.1a. IMPROVE 2016–2019 $PM_{2.5}$ reconstructed ambient annual mean light extinction coefficients for ammonium sulfate (b_{ext_AS}, Mm^{-1}). Wavelength corresponds to 550 nm.

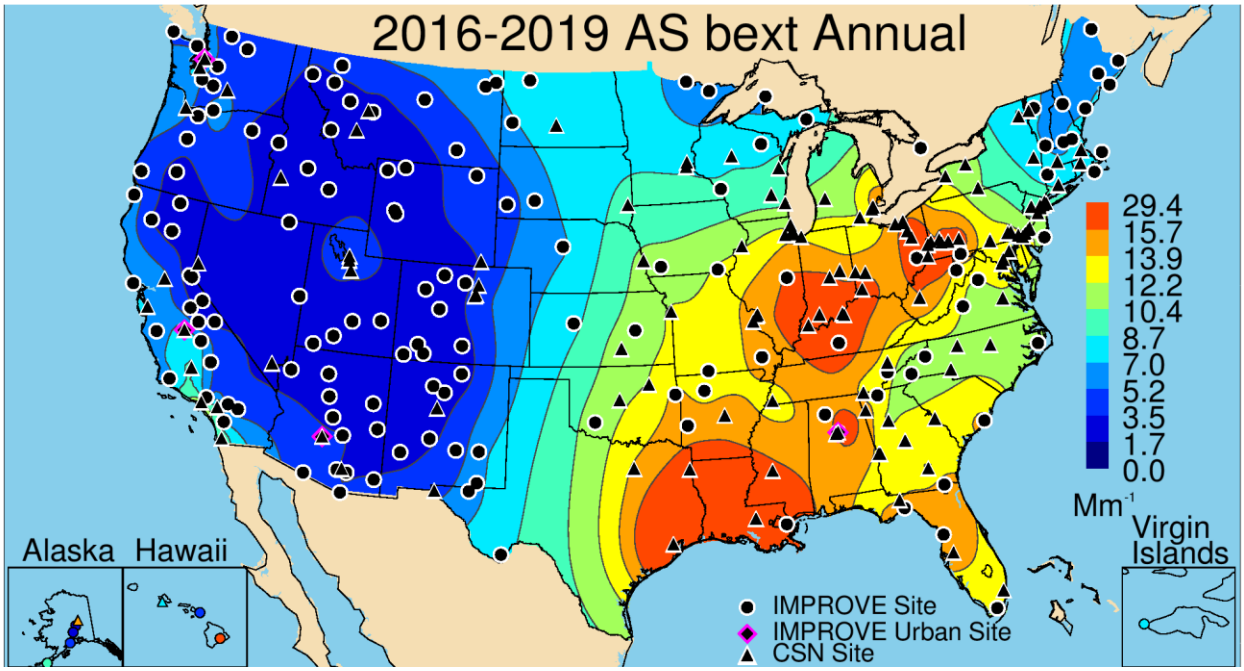

Figure 4.2.1b. IMPROVE and CSN 2016–2019 $PM_{2.5}$ reconstructed ambient annual mean light extinction coefficients for ammonium sulfate (b_{ext_AS}, Mm^{-1}). Wavelength corresponds to 550 nm.

At sites in the eastern United States, the IMPROVE annual mean fractional contribution of b_{ext_AS} to reconstructed b_{ext_aer} ranged between 0.3 and 0.5 (Figure 4.2.1c), with the highest contributions at sites in the East along the Ohio River valley and the Southeast. Contributions decreased toward the West, with contributions around 0.25–0.30 across the central United States. The spatial pattern generally followed that of b_{ext_AS}. The lowest contributions occurred at sites

in northern California, Idaho, and Oregon (<0.15). The sites with the highest contributions of b_{ext_AS} were Hawaii Volcanoes NP, Hawaii (0.76, HAVO1), Breton Island, Louisiana (0.48, BRIS1), and Dolly Sods Wilderness Area (WA), West Virginia (0.47, DOSO1). The minimum contributions occurred at Nogales, Arizona (0.08, NOGA1) and Sawtooth NF, Idaho (0.09, SAWT1).

The fractional contribution of b_{ext_AS} at the CSN sites ranged from 0.06 (Butte, Montana, 300930005) to 0.42 (Capitol, Louisiana, 220330009), with very similar spatial patterns as the IMPROVE network (Figure 4.2.1d). However, the addition of CSN sites often corresponded to lower contributions. For example, sites in the eastern United States showed lower contributions, especially at urban sites across the Southeast (~0.3). Lower contributions also occurred for urban sites around the Great Lakes, central United States, and urban sites across the West (e.g., Colorado, New Mexico, Arizona, Idaho, Montana, and California), likely due to the importance of the contribution of other species to b_{ext_aer}, such as b_{ext_POM} and b_{ext_AN}.

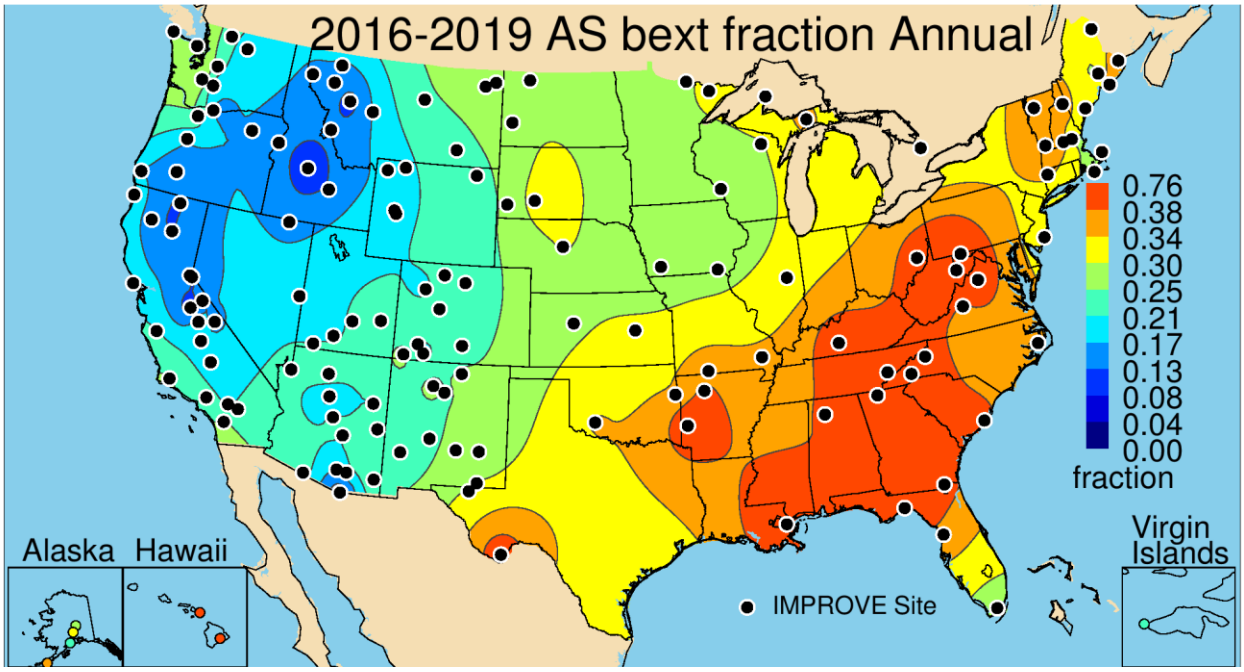

Figure 4.2.1c. IMPROVE 2016–2019 annual mean fraction contributions of ambient ammonium sulfate light extinction coefficient (b_{ext_AS}) to reconstructed aerosol b_{ext}. Wavelength corresponds to 550 nm.

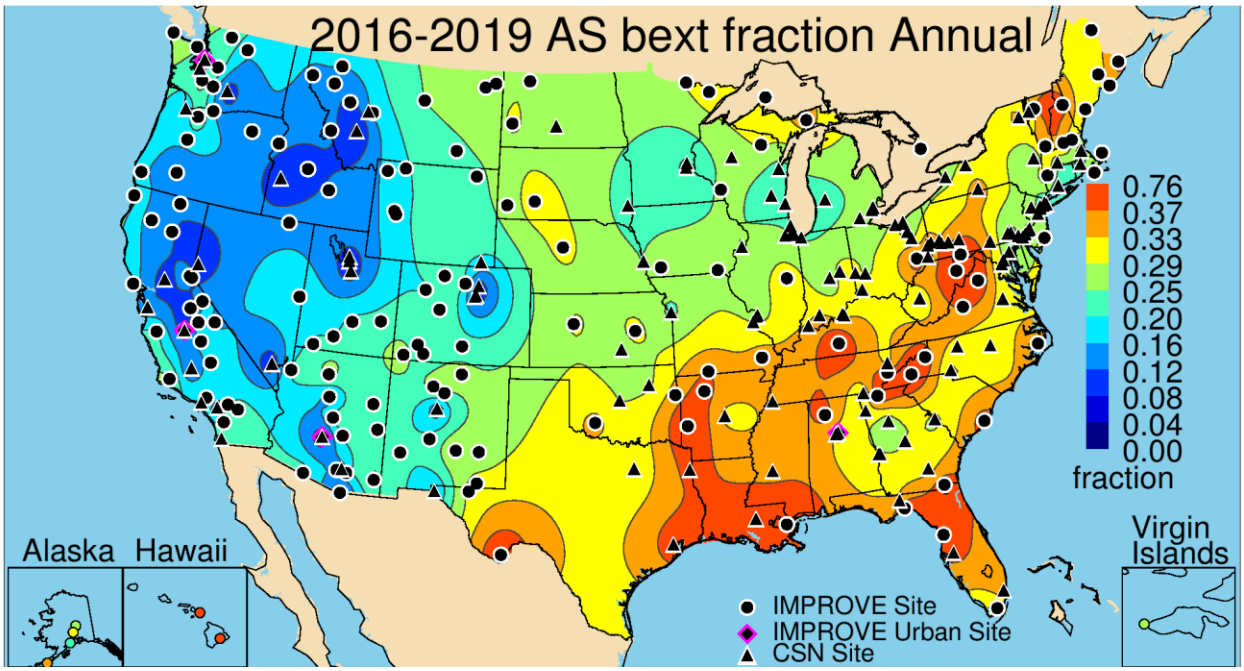

Figure 4.2.1d. IMPROVE and CSN 2016–2019 annual mean fraction contributions of ambient ammonium sulfate light extinction coefficient (b_{ext_AS}) to reconstructed aerosol b_{ext}. Wavelength corresponds to 550 nm.

4.2.2 $PM_{2.5}$ Ammonium Nitrate Light Extinction Coefficients

The spatial pattern of the 2016–2019 rural IMPROVE annual mean AN light extinction coefficients (b_{ext_AN}; Figure 4.2.2a) was similar to the annual mean AN mass concentration pattern (Chapter 2). Rural IMPROVE estimates ranged from 0.34 Mm^{-1} at Denali NP, Alaska (DENA1), and 0.49 Mm^{-1} at Sawtooth NF, Idaho (SAWT1), to 19.37 Mm^{-1} in Bondville, Illinois (BOND1), located in the agricultural Midwest. The BOND1 site is in the center of the area of highest b_{ext_AN} located in the central United States, where annual mean b_{ext_AN} was typically greater than 10 Mm^{-1}. In general, however, most of the rural sites corresponded to low annual mean b_{ext_AN} (<5 Mm^{-1}), except at the Columbia River Gorge (CORI1) site in Washington (14.74 Mm^{-1}) and sites in northern North Dakota and Montana (~7 Mm^{-1}) near oil and gas development activity. Somewhat elevated levels of b_{ext_AN} also occurred at sites along the West Coast (~5 Mm^{-1}).

Annual mean b_{ext_AN} at CSN sites ranged from 1.25 Mm^{-1} in Kapolei, Hawaii (150030010) and 2.06 Mm^{-1} at Tucson, Arizona (040191028) to 34.08 Mm^{-1} in Bakersfield, California (060290014). The spatial pattern of b_{ext_AN} with CSN sites was similar to that of annual mean AN mass concentrations, with a region of high extinction in the central United States and hot spots of high b_{ext_AN} at western sites in Utah, Washington, and the Central Valley of California (Figure 4.2.2b). CSN sites in the southeastern United States were relatively low (<10 Mm^{-1}).

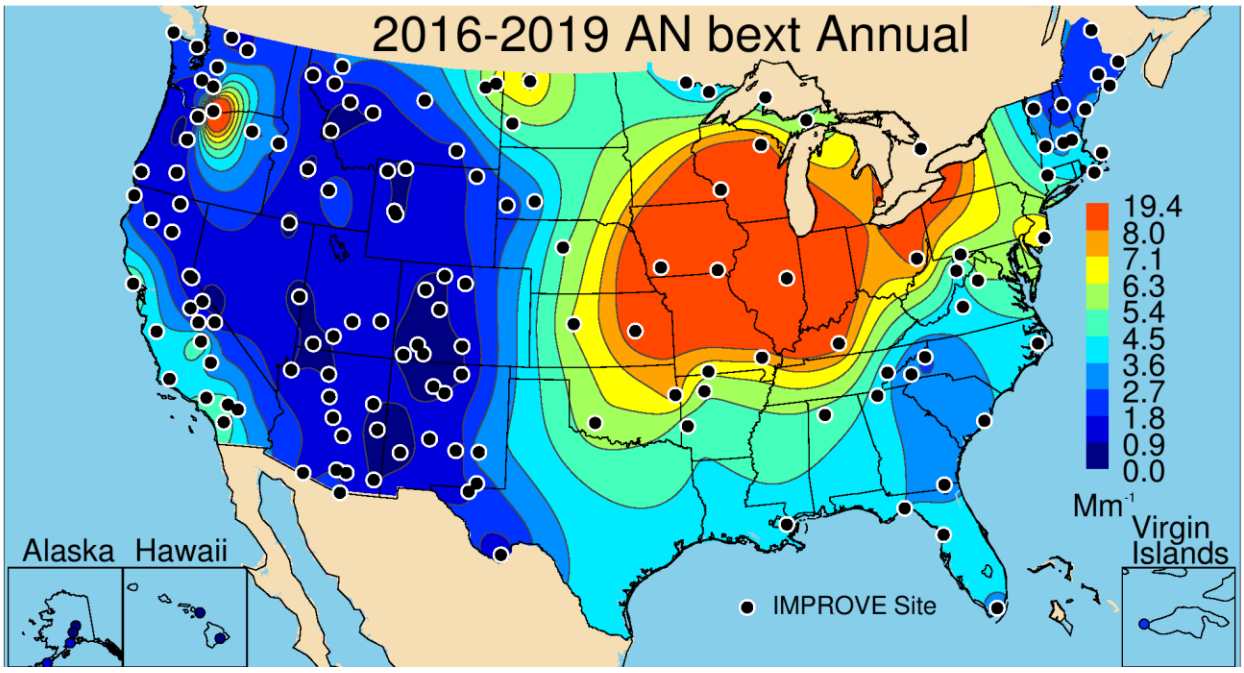

Figure 4.2.2a. IMPROVE 2016–2019 $PM_{2.5}$ reconstructed ambient annual mean light extinction coefficients for ammonium nitrate (b_{ext_AN}, Mm^{-1}). Wavelength corresponds to 550 nm.

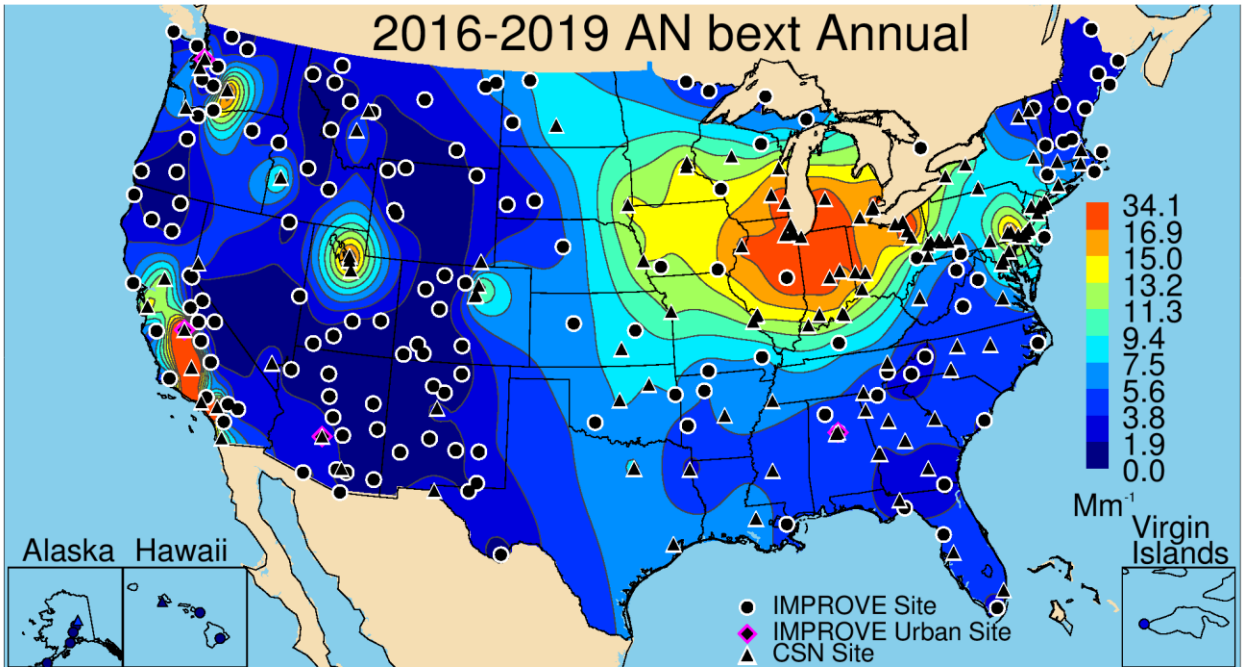

Figure 4.2.2b. IMPROVE and CSN 2016–2019 $PM_{2.5}$ reconstructed ambient annual mean light extinction coefficients for ammonium nitrate (b_{ext_AN}, Mm^{-1}). Wavelength corresponds to 550 nm.

The spatial pattern of the annual mean fractional contributions of IMPROVE b_{ext_AN} to b_{ext_aer} reflects the b_{ext_AN} pattern (see Figure 4.2.2c), with elevated fractional contributions (>0.3) of b_{ext_AN} to b_{ext_aer} in areas of high agricultural activity in the central United States. Sites in Southern California and the Central Valley had contributions near 0.2. Contributions of b_{ext_AN} to b_{ext_aer} were somewhat higher at sites in northern North Dakota and Montana (~0.25). However,

most sites in the Intermountain West corresponded to low annual mean contributions (<0.1), as did sites in the southeastern United States. The highest annual mean fractional contribution occurred at Bondville, Illinois (0.38, BOND1), and the lowest occurred at Sawtooth NF, Idaho (0.03, SAWT1).

The addition of CSN sites did not significantly alter the spatial patterns in annual mean b_{ext_AN} contributions to b_{ext_aer} (Figure 4.2.2d), with a region of high fractional contribution in the central United States. However, additional impacts at urban sites created hot spots (>0.3), such as at sites in the Colorado Front Range and around Salt Lake City, Utah, as well as the Central Valley of California. The highest annual mean fractional contribution of b_{ext_AN} to b_{ext_aer} occurred in Bountiful, Utah (0.44, 490110004), compared to the lowest in General Coffee, Georgia (0.06, 130690002).

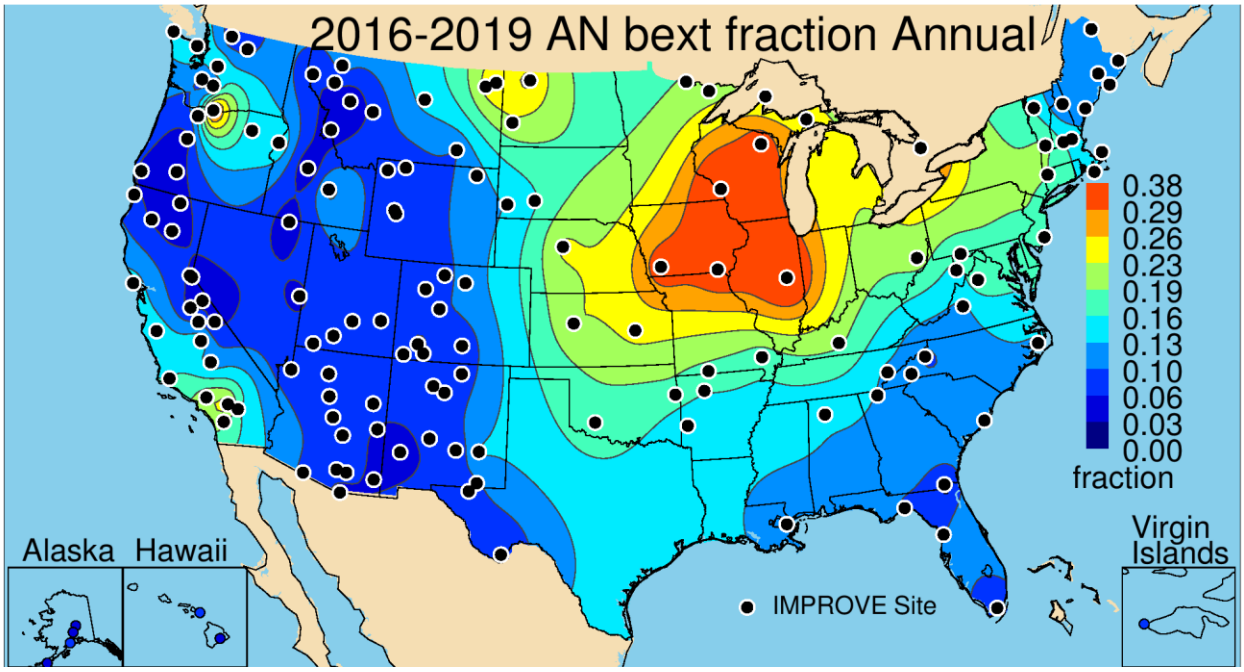

Figure 4.2.2c. IMPROVE 2016–2019 annual mean fraction contributions of ambient ammonium nitrate light extinction coefficient (b_{ext_AN}) to reconstructed aerosol b_{ext}. Wavelength corresponds to 550 nm.

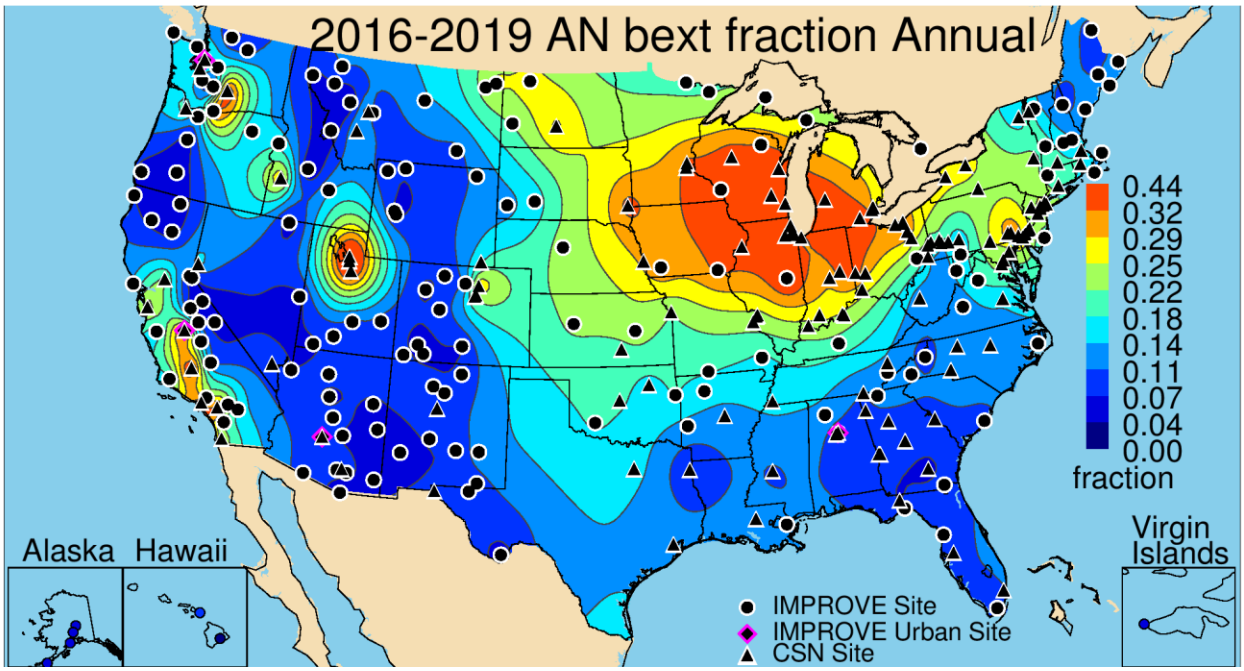

Figure 4.2.2d. IMPROVE and CSN 2016–2019 annual mean fraction contributions of ambient ammonium nitrate light extinction coefficient (b_{ext_AN}) to reconstructed aerosol b_{ext}. Wavelength corresponds to 550 nm.

4.2.3 $PM_{2.5}$ Particulate Organic Matter Light Extinction Coefficients

The 2016–2019 IMPROVE annual mean light extinction coefficient due to POM (b_{ext_POM}) ranged from 0.60 Mm^{-1} in Haleakala Crater NP, Hawaii (HACR1), and 2.95 Mm^{-1} in White River NF, Colorado (WHRI1), to 27.01 Mm^{-1} in Yosemite NP, California (YOSE1). POM was considered nonhygroscopic in equation (4.4), so the spatial pattern of b_{ext_POM} (Figure 4.2.3a) reflects that of the POM annual mean mass concentration pattern. High levels of b_{ext_POM} were observed at sites in the southern and southeastern United States. Regions of the northwestern United States also included sites with relatively high b_{ext_POM}, such as the Central Valley of California (10–15 Mm^{-1} and higher). Sites in northern Idaho and Montana also had high b_{ext_POM}, likely associated with biomass burning impacts. Low b_{ext_POM} occurred at sites across the southwestern United States and part of the Intermountain West, with values less than 5 Mm^{-1}.

Urban annual mean b_{ext_POM} was higher than at rural sites. Values ranged from 1.66 Mm^{-1} in Kapolei, Hawaii (150030010), and 6.06 Mm^{-1} at the base of Whiteface Mountain, New York (360310003), to 24.04 Mm^{-1} in Fresno, California (020190011). Other urban sites in the Central Valley of California had annual mean b_{ext_POM} over 15 Mm^{-1}. Elevated b_{ext_POM} was also observed at sites in the southeastern United States. Stronger gradients near cities were observed with the inclusion of CSN data, suggesting local urban sources of organic aerosols. Regional sources (perhaps biogenic or wildfire emissions) seemed more spatially extensive in the southeastern United States, compared to more localized sources for many urban centers in the West, such as the Front Range of Colorado; Phoenix, Arizona; and Las Vegas, Nevada.

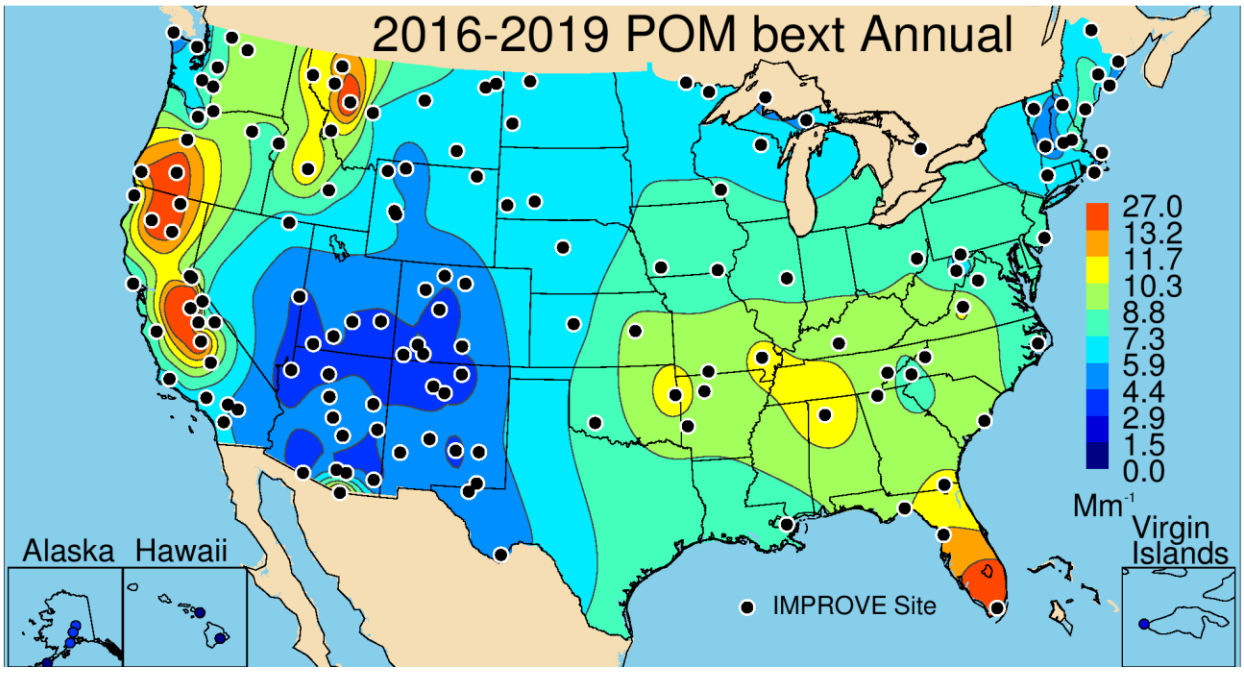

Figure 4.2.3a. IMPROVE 2016–2019 $PM_{2.5}$ reconstructed ambient annual mean light extinction coefficients for particulate organic matter (b_{ext_POM}, Mm^{-1}). Wavelength corresponds to 550 nm.

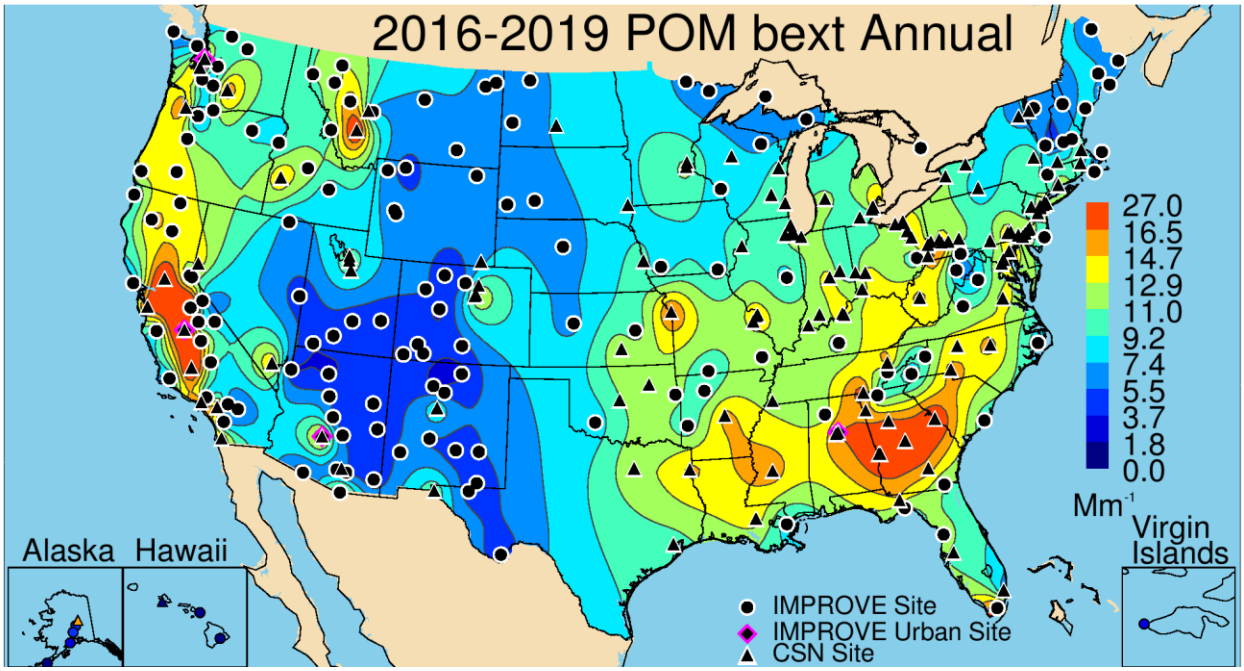

Figure 4.2.3b. IMPROVE and CSN 2016–2019 $PM_{2.5}$ reconstructed ambient annual mean light extinction coefficients for particulate organic matter (b_{ext_POM}, Mm^{-1}). Wavelength corresponds to 550 nm.

The IMPROVE fractional contribution of b_{ext_POM} to b_{ext_aer} is presented in Figure 4.2.3c. Contributions of 0.5 or higher were observed at sites in the western United States, especially in northern California, southern Oregon, Idaho, and Montana, suggesting the strong impact of biomass burning emissions to b_{ext_aer}. The east–west gradient observed for fractional b_{ext_POM} shows lower fractions in the eastern United States (<0.3), a gradient mirroring that observed for

b_{ext_AS}. The maximum annual mean fractional contribution occurred at Sawtooth NF, Idaho (0.70, SAWT1), compared to the lowest at Hawaii Volcano NP, Hawaii (0.05, HAVO1), and Martha's Vineyard, Massachusetts (0.16, MAVI1).

A similar pattern was observed with the addition of the CSN sites, with higher fractional contributions at sites in the West (Figure 4.2.3d). Interestingly, urban sites in Utah had lower fractional contributions compared to surrounding areas, likely because of the contribution from b_{ext_AN} to b_{ext_aer} (see Figure 4.2.2d) at these sites. The lowest annual mean fractional contributions corresponded to sites in the central United States, also likely due to the role of b_{ext_AN}. CSN sites in the southeastern United States had higher fractional contributions (0.35–0.4) relative to surrounding areas. The fractional contribution ranged from 0.17 (Davie, Florida, 120110034) to 0.49 in Butte, Montana (300930005).

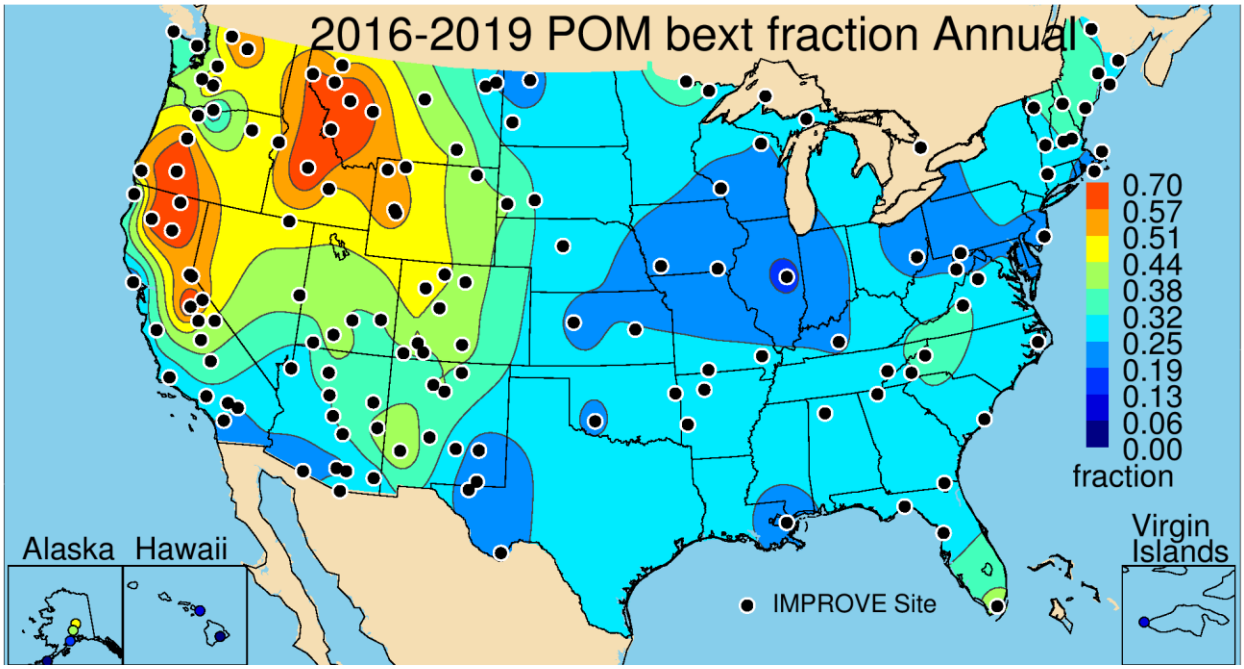

Figure 4.2.3c. IMPROVE 2016–2019 annual mean fraction contributions of particulate organic matter light extinction coefficient (b_{ext_POM}) to reconstructed aerosol b_{ext}. Wavelength corresponds to 550 nm.

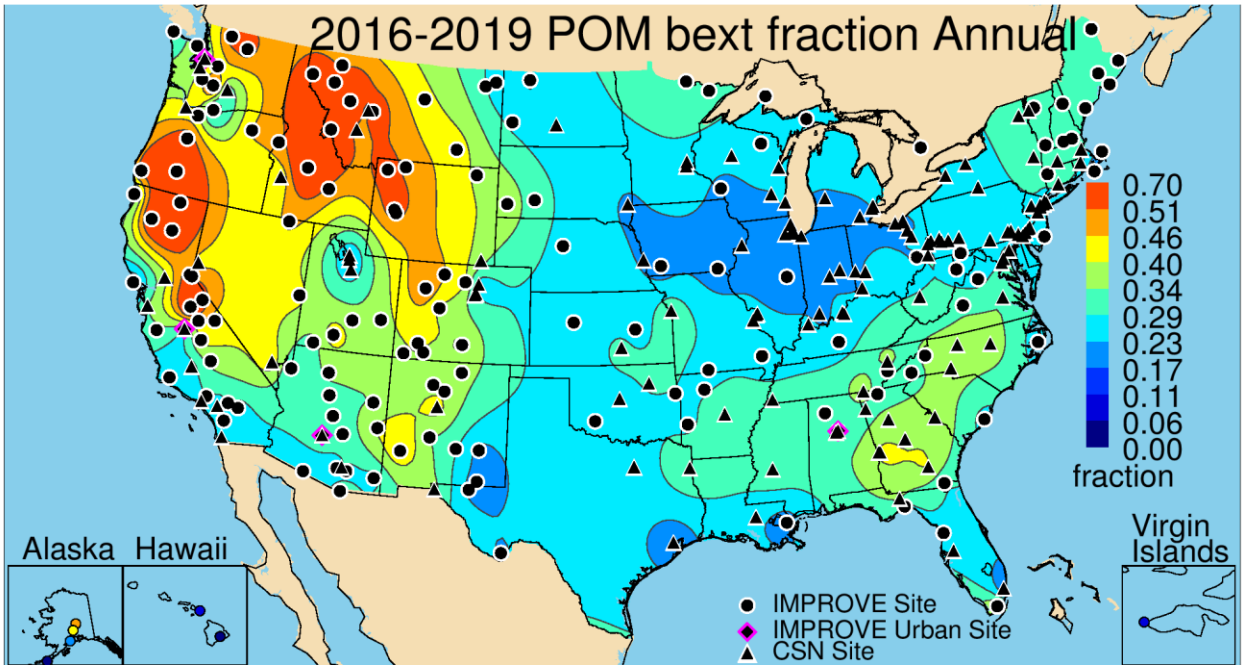

Figure 4.2.3d. IMPROVE and CSN 2016–2019 annual mean fraction contributions of particulate organic matter light extinction coefficient (b_{ext_POM}) to reconstructed aerosol b_{ext}. Wavelength corresponds to 550 nm.

4.2.4 $PM_{2.5}$ Elemental Carbon Light Extinction Coefficients

The IMPROVE spatial pattern of 2016–2019 annual mean EC extinction coefficients (b_{ext_EC}) was similar to the EC mass concentration patterns, with elevated levels at eastern sites (Figure 4.2.4a). The maximum annual mean b_{ext_EC} (8.86 Mm^{-1}) occurred at Nogales, Arizona (NOGA1), and at Chassahowitzka NWR (3.37 Mm^{-1}, CHAS1) in Florida, similar to the high EC mass concentrations. The lowest b_{ext_EC} occurred at Haleakala Crater NP, Hawaii (0.15 Mm^{-1} HACR1), and White River Face NF, Colorado (0.59 Mm^{-1}, WHRI1). These sites also had the lowest annual mean b_{ext_POM}. The highest b_{ext_EC} occurred at sites across the eastern United States and some sites in the Northwest, while sites in the southwestern United States and Intermountain West had values less than 2 Mm^{-1}. Most (93%) IMPROVE sites corresponded to very low (<3 Mm^{-1}) b_{ext_EC}.

Impacts of urban sources on b_{ext_EC} was evident from the strong gradients surrounding urban sites, such as the Front Range of Colorado; Phoenix, Arizona; Las Vegas, Nevada; and sites in the Central Valley of California (Figure 4.2.4b). Elevated b_{ext_EC} also occurred at sites along the Ohio River valley and at sites in Alabama and Georgia., The minimum annual mean urban b_{ext_EC} (0.96 Mm^{-1}) occurred at Kapolei, Hawaii (150030010), and Whiteface Mountain Base, New York (1.17 Mm^{-1}, 360310003). The maximum CSN annual mean b_{ext_EC} occurred at Liberty, Pennsylvania (14.26 Mm^{-1}, 420030064).

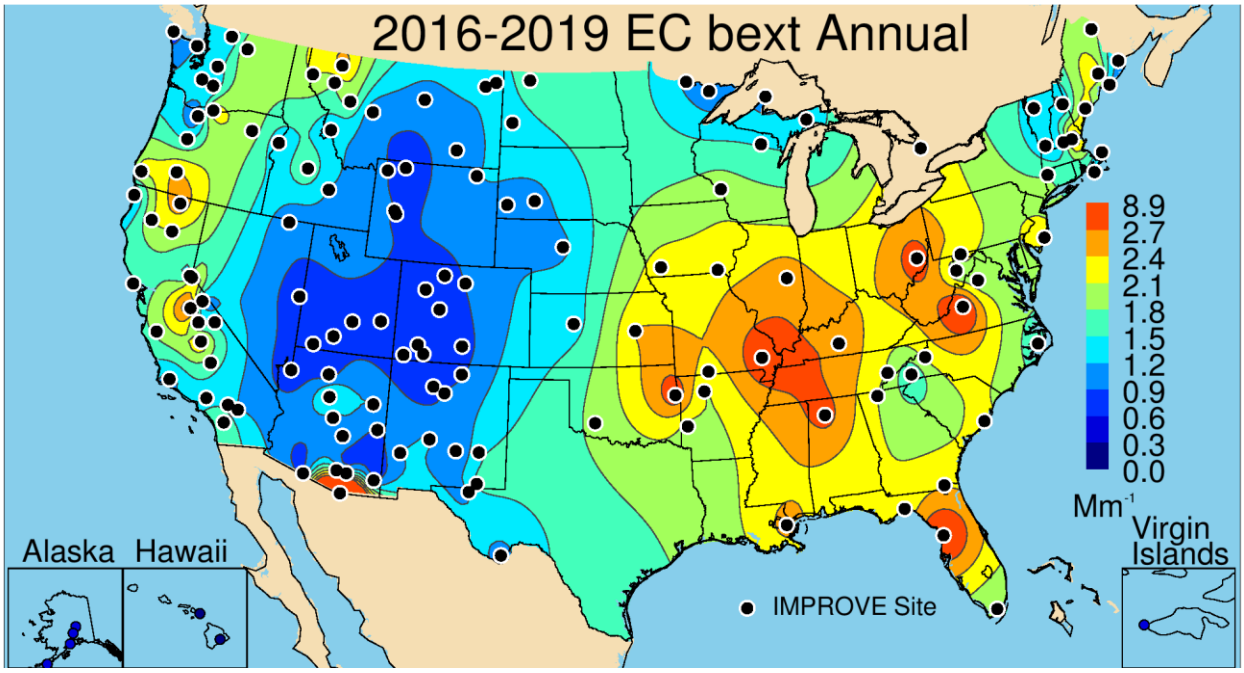

Figure 4.2.4a. IMPROVE 2016–2019 $PM_{2.5}$ reconstructed ambient annual mean light extinction coefficients for elemental carbon (b_{ext_EC}, Mm^{-1}). Wavelength corresponds to 550 nm.

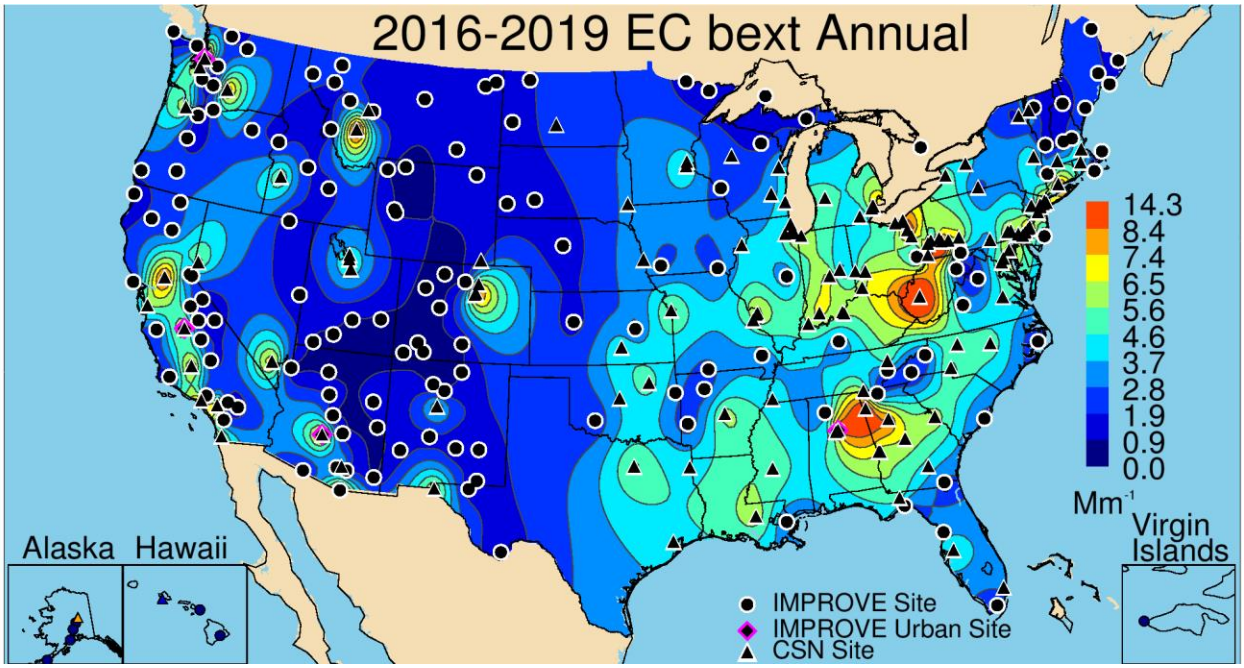

Figure 4.2.4b. IMPROVE and CSN 2016–2019 $PM_{2.5}$ reconstructed ambient annual mean light extinction coefficients for elemental carbon (b_{ext_EC}, Mm^{-1}). Wavelength corresponds to 550 nm.

The IMPROVE annual mean fractional contribution of b_{ext_EC} to b_{ext_aer} ranged from 0.01 at Hawaii Volcanoes NP, Hawaii (HAVO1), and 0.04 at Redwood NP, California (REDW1), to 0.13 at Lake Tahoe Community College, California (LTCC1), and 0.19 at Nogales, Arizona (NOGA). Most of the IMPROVE sites corresponded to contributions of 0.05 or greater (Figure 4.2.4c). The sites with highest contributions were in the northwestern United States, the

Intermountain West, and the southwestern United States. Sites in the northeastern United States, Ohio River valley, and Appalachian Mountain region were also associated with elevated contributions.

Localized urban impacts on the fractional contribution of b_{ext_EC} on b_{ext_aer} were clear from the tight gradients surrounding several urban sites in Figure 4.2.4d. Many of the same sites with elevated b_{ext_EC} also corresponded to high fractional contributions, such as around the Front Range of Colorado; Butte, Montana; El Paso, Texas; Las Vegas, Nevada, and others. Sites in Alabama, Georgia, and West Virginia also had elevated contributions. The minimum annual mean contribution was 0.06 at Whiteface Mountain Base, New York (360310003), compared to the maximum of 0.25 at Butte, Montana (300930005).

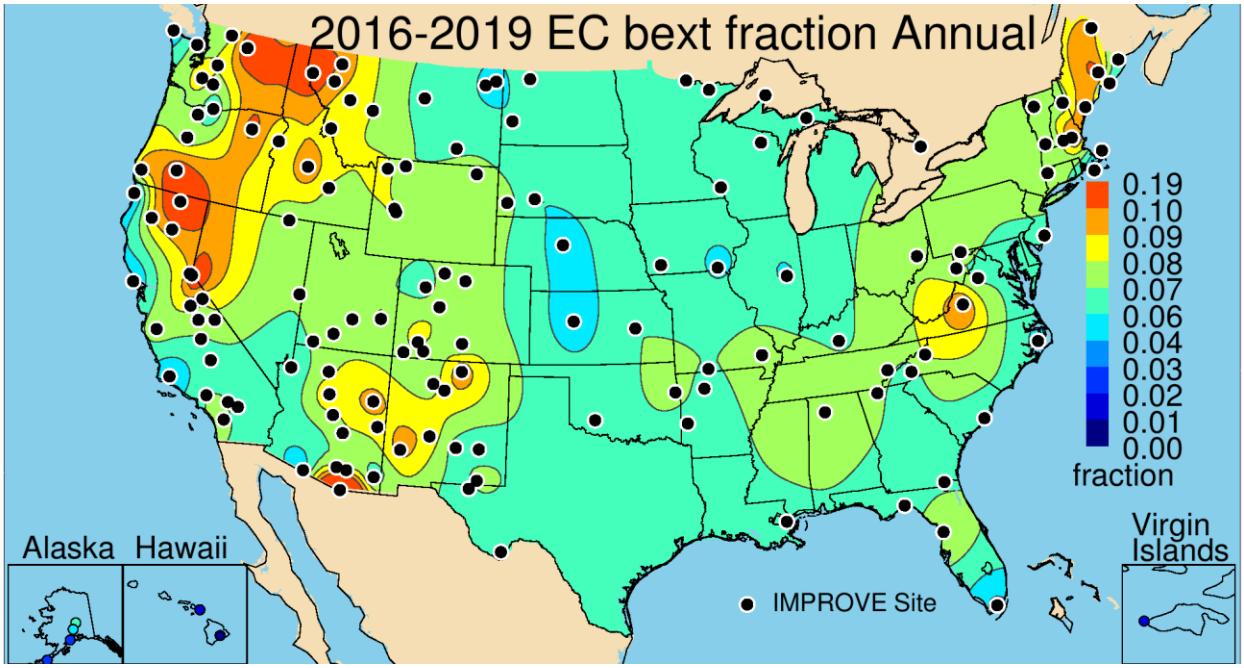

Figure 4.2.4c. IMPROVE 2016–2019 annual mean fraction contributions of elemental carbon light extinction coefficient (b_{ext_EC}) to reconstructed aerosol b_{ext}. Wavelength corresponds to 550 nm.

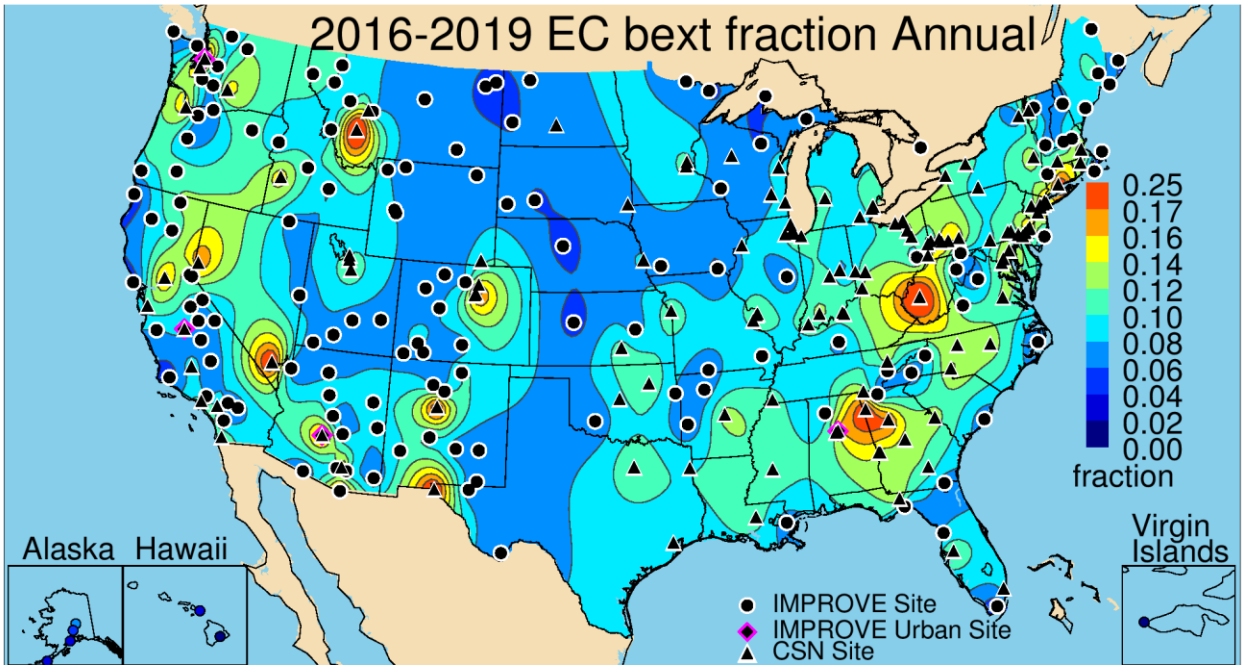

Figure 4.2.4d. IMPROVE and CSN 2016–2019 annual mean fraction contributions of elemental carbon light extinction coefficient (b_{ext_EC}) to reconstructed aerosol b_{ext}. Wavelength corresponds to 550 nm.

4.2.5 $PM_{2.5}$ Fine Dust Light Extinction Coefficients

The annual mean FD b_{ext} (b_{ext_FD}) spatial pattern (Figure 4.2.5a) was the same as the FD mass concentration pattern. The rural IMPROVE annual mean b_{ext_FD} ranged from 0.07 Mm^{-1} in the Makah Tribe site in Washington (MAKA2) to 3.10 Mm^{-1} in Sycamore Canyon, Arizona (SYCA2). The highest b_{ext_FD} (~1-3 Mm^{-1}) occurred at sites in the southwestern United States, with a lobed spatial pattern that followed the Mogollon Plateau. Somewhat higher values extended to sites northward and into the southeastern United States. The Virgin Islands NP (VIIS1) site also had high b_{ext_FD} (1.95 Mm^{-1}), likely due to impacts of North African dust transport. Sites in the northwestern and northeastern United States had relatively low b_{ext_FD} (<0.5 Mm^{-1}).

The addition of data from CSN sites provided further detail to the spatial pattern of b_{ext_FD} (Figure 4.2.5b) but did not alter it substantially. Recall the bias in FD between IMPROVE and CSN sites discussed in Chapter 1, with higher IMPROVE FD concentrations. However, even with this bias, hot spots (1–2 Mm^{-1}) of annual mean b_{ext_FD} for CSN sites occurred at sites around the Front Range of Colorado; Salt Lake City, Utah; the Central Valley of California; Birmingham, Alabama; Dallas, Texas; and St. Louis, Missouri, among others. Annual mean values ranged between the minimum of 0.17 Mm^{-1} at the Pinnacle SP site in New York (361010003) to 2.07 Mm^{-1} in El Paso, Texas (481410044).

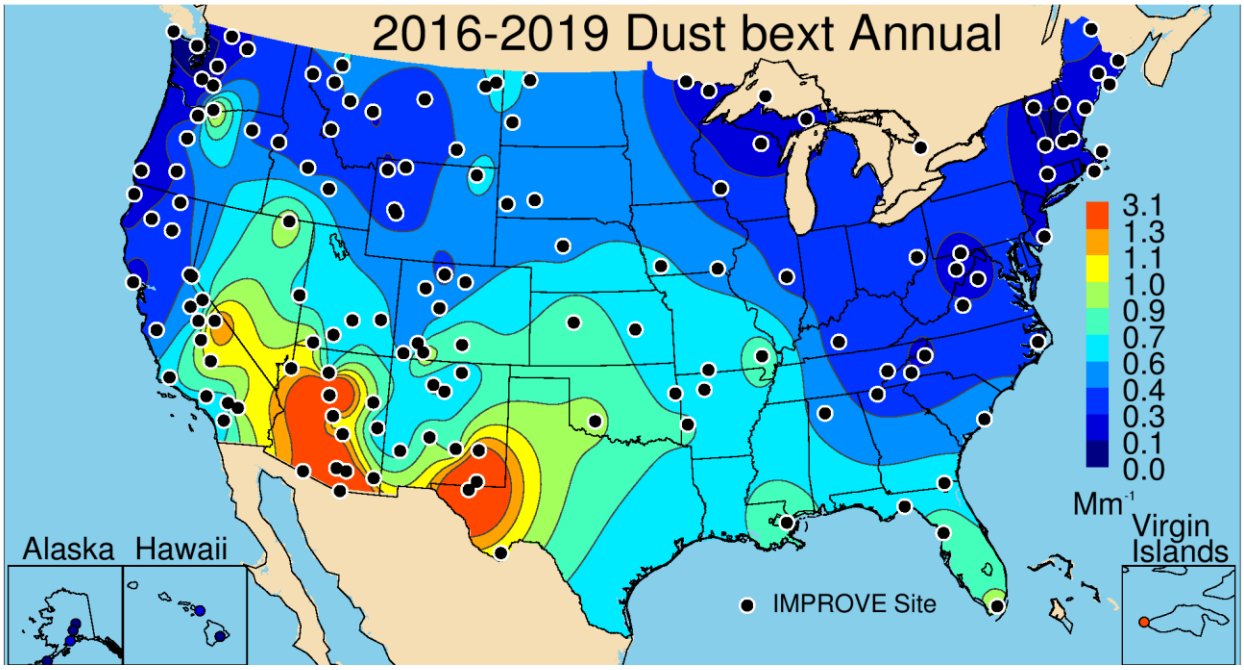

Figure 4.2.5a. IMPROVE 2016–2019 $PM_{2.5}$ reconstructed ambient annual mean light extinction coefficients for fine dust (b_{ext_FD}, Mm^{-1}). Wavelength corresponds to 550 nm.

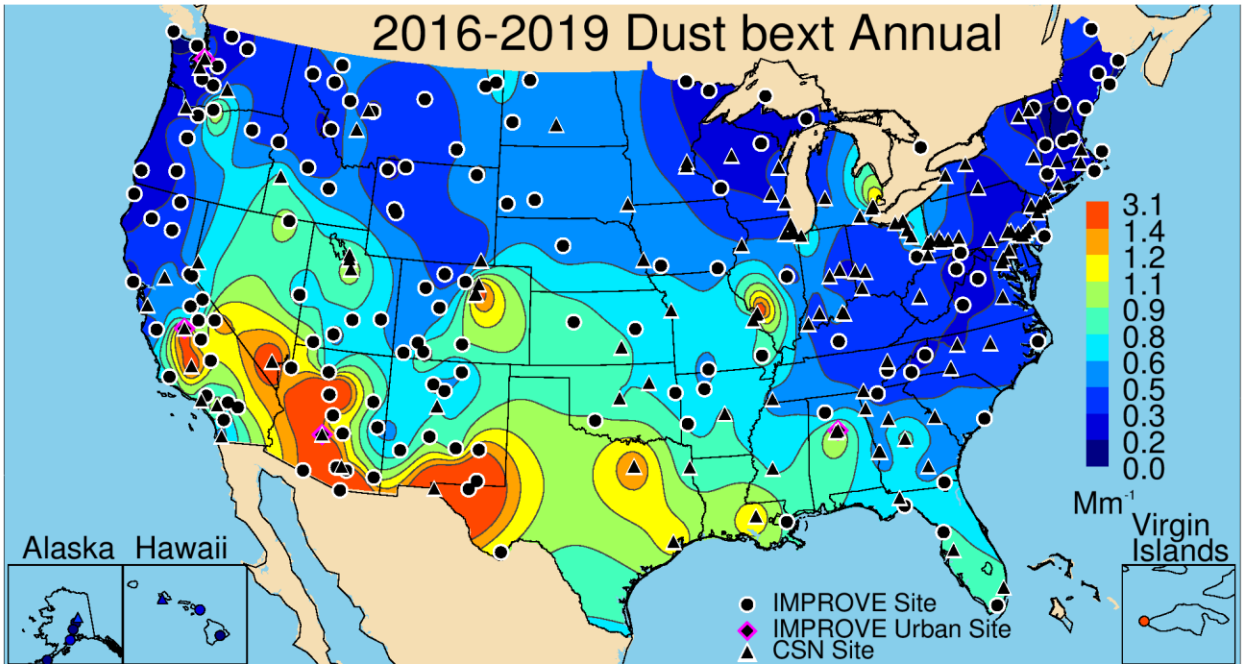

Figure 4.2.5b. IMPROVE and CSN 2016–2019 $PM_{2.5}$ reconstructed ambient annual mean light extinction coefficients for fine dust (b_{ext_FD}, Mm^{-1}). Wavelength corresponds to 550 nm.

The largest b_{ext_FD} annual mean fractional contributions to b_{ext_aer} occurred at sites in the southwestern United States (Figure 4.2.5c), with values around 0.10–0.15. Fractional contributions ranged from 0.004 in Simeonof, Alaska (SIME1), and 0.005 at both the Makah Tribe site (MAKA2) in Washington and the Redwood NP site in California (REDW1) to 0.16 at Sycamore Canyon, Arizona (SYCA2). Most sites of the eastern United States corresponded to annual mean contributions less than 0.03.

The spatial pattern in fractional contribution of b_{ext_FD} to b_{ext_aer} did not change substantially with the addition of CSN sites (Figure 4.2.5d). The highest contributions occurred at sites in the southwestern United States, while fractional contributions at sites across the eastern United States and along the West Coast were low (~0.02 or below). The minimum annual mean contribution was 0.005 at Five Points, Ohio (391530023), and the maximum contribution was 0.07 in El Paso, Texas (481410044). No CSN sites had contributions greater than 0.1.

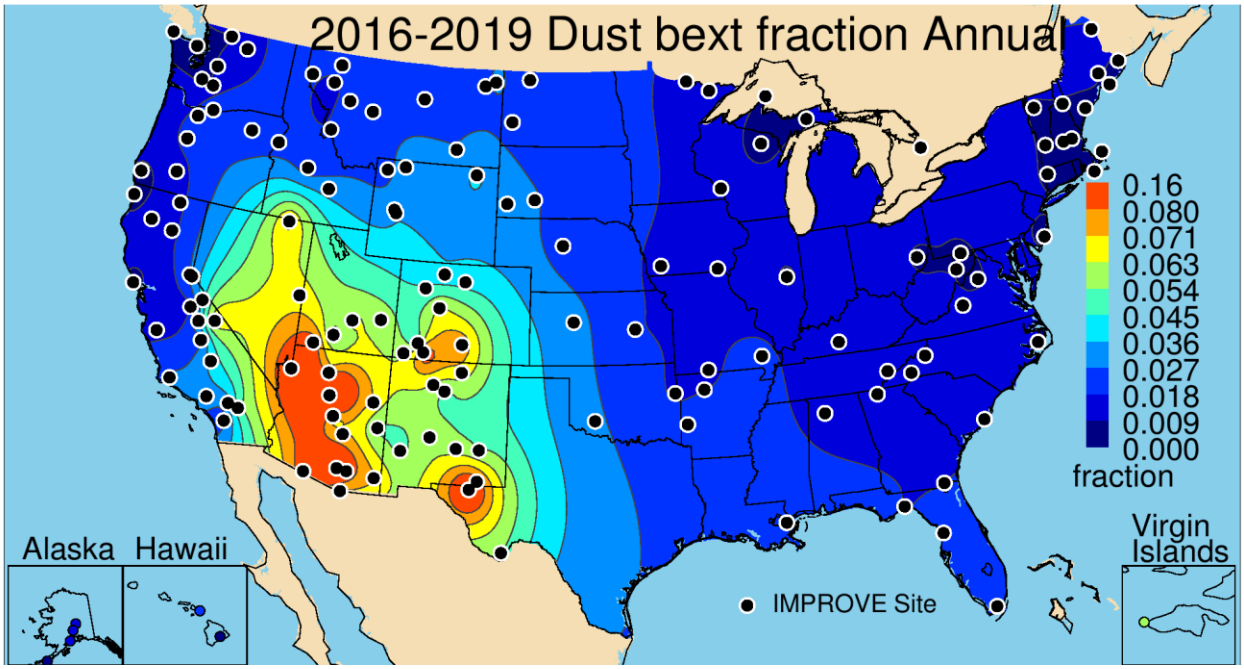

Figure 4.2.5c. IMPROVE 2016–2019 annual mean fraction contributions of fine dust light extinction coefficient (b_{ext_FD}) to reconstructed aerosol b_{ext}. Wavelength corresponds to 550 nm.

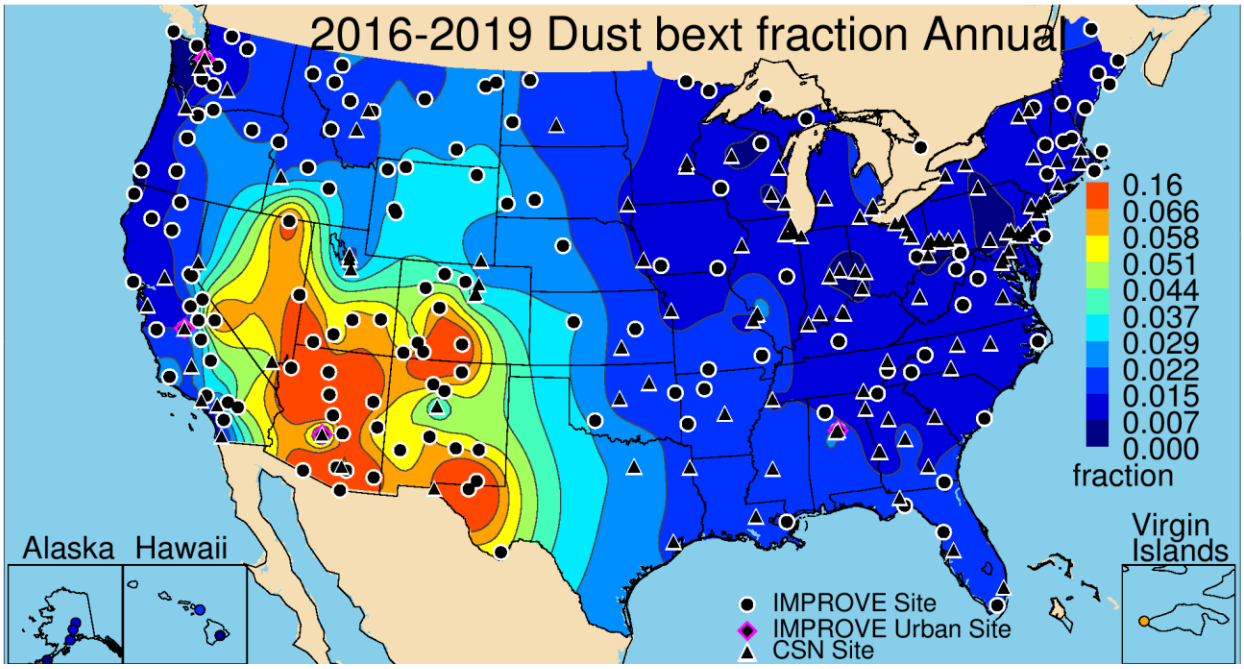

Figure 4.2.5d. IMPROVE and CSN 2016–2019 annual mean fraction contributions of fine dust light extinction coefficient (b_{ext_FD}) to reconstructed aerosol b_{ext}. Wavelength corresponds to 550 nm.

4.2.6 $PM_{2.5}$ Sea Salt Extinction Coefficients

Spatial patterns of IMPROVE 2016–2019 monthly mean SS light extinction coefficients (b_{ext_SS}) were highest along the coasts (Figure 4.2.6a) and at sites in Alaska, Hawaii, and the Virgin Islands. Annual mean values were extremely low across the western United States (<0.3 Mm^{-1}) and at sites along the Appalachian Mountains. Values ranged from 0.04 Mm^{-1} in North Absaroka, Wyoming (NOAB1), to 12.73 Mm^{-1} in Point Reyes National Seashore (NS), California (PORE1).

The coastal pattern of elevated b_{ext_SS} was also observed with the inclusion of CSN sites (Figure 4.2.6b); however, recall the bias between IMPROVE and CSN SS estimates at collocated sites, with IMPROVE yielding higher concentrations. The maximum b_{ext_SS} occurred at Kapolei, Hawaii (4.47 Mm^{-1}, 150030010), and Davie, Florida (3.46 Mm^{-1}, 120110034), and the minimum b_{ext_SS} occurred at Pinnacle SP, New York (0.00 Mm^{-1}, 361010003).

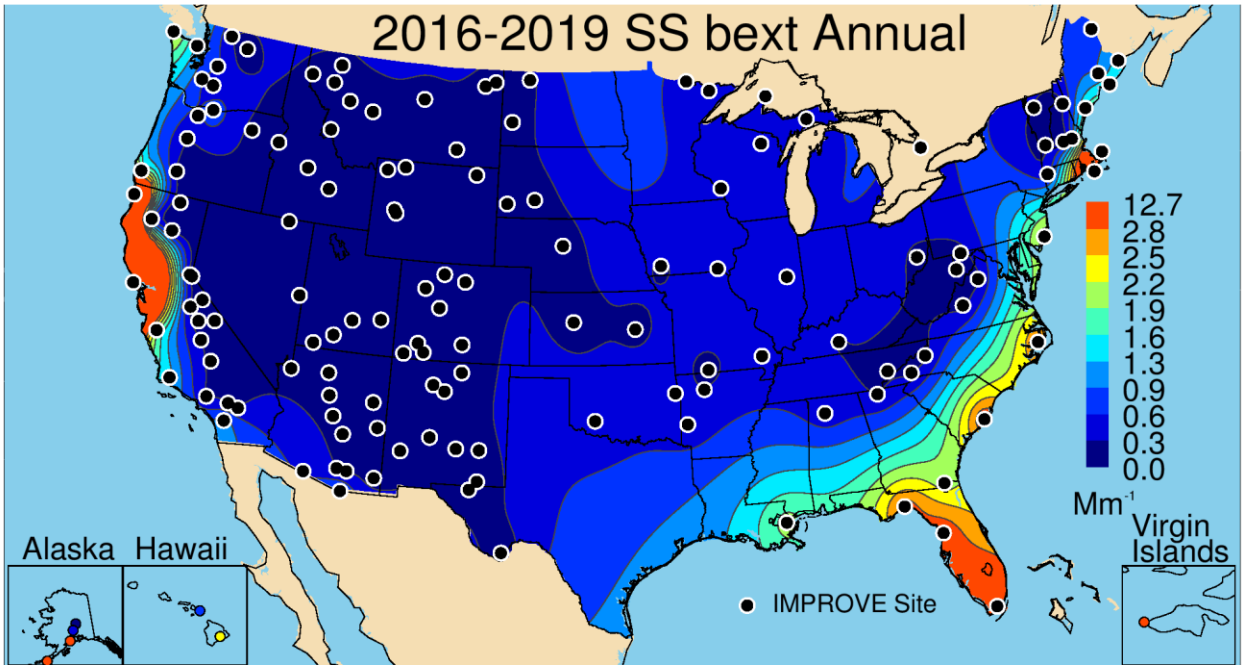

Figure 4.2.6a. IMPROVE 2016–2019 $PM_{2.5}$ reconstructed ambient annual mean light extinction coefficients for sea salt (b_{ext_SS}, Mm^{-1}). Wavelength corresponds to 550 nm.

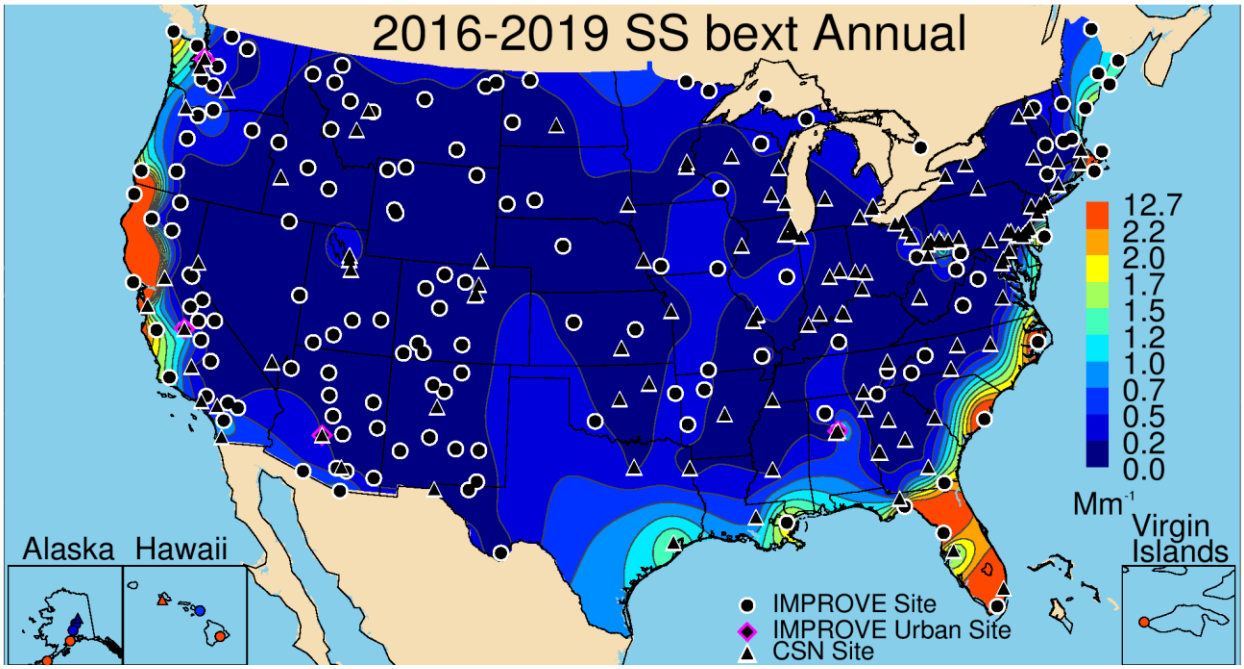

Figure 4.2.6b. IMPROVE and CSN 2016–2019 $PM_{2.5}$ reconstructed ambient annual mean light extinction coefficients for sea salt (b_{ext_SS}, Mm^{-1}). Wavelength corresponds to 550 nm.

The IMPROVE fractional contribution of b_{ext_SS} to b_{ext_aer} was low on an annual mean basis, except at coastal sites where the maximum IMPROVE contribution (0.41) occurred at Simeonof, Alaska (SIME1), and Point Reyes NS, California (PORE1, 0.33) (Figure 4.2.6c). Relatively high annual mean contributions also occurred at Redwood NP, California (0.31, REDW1), and Virgin Islands NP (0.28, VIIS1). However, most sites corresponded to contributions less than 0.05. The lowest contribution of SS to b_{ext_aer} (0.003) occurred at both Monture, Montana (MONT1), and Thunder Basin, Wyoming (THBA1).

The largest annual mean fractional contribution for the CSN occurred at Davie, Florida (0.09, 120110034). No other sites had contributions greater than 0.05 (Figure 4.2.6d). Sites in Hawaii or Alaska were missing from fractional contribution analysis because other species were missing. The lowest fractional contribution occurred at Cheyenne, Wyoming (0.00, 560210100).

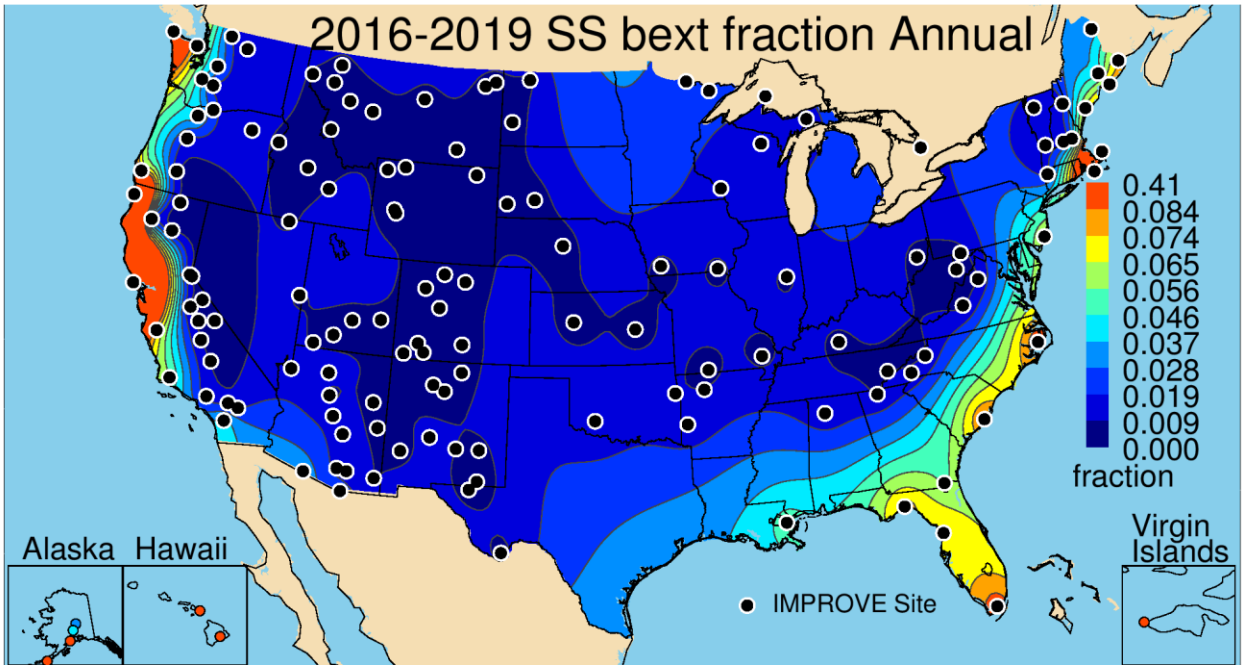

Figure 4.2.6c. IMPROVE 2016–2019 annual mean fraction contributions of sea salt light extinction coefficient (b_{ext_SS}) to reconstructed aerosol b_{ext}. Wavelength corresponds to 550 nm.

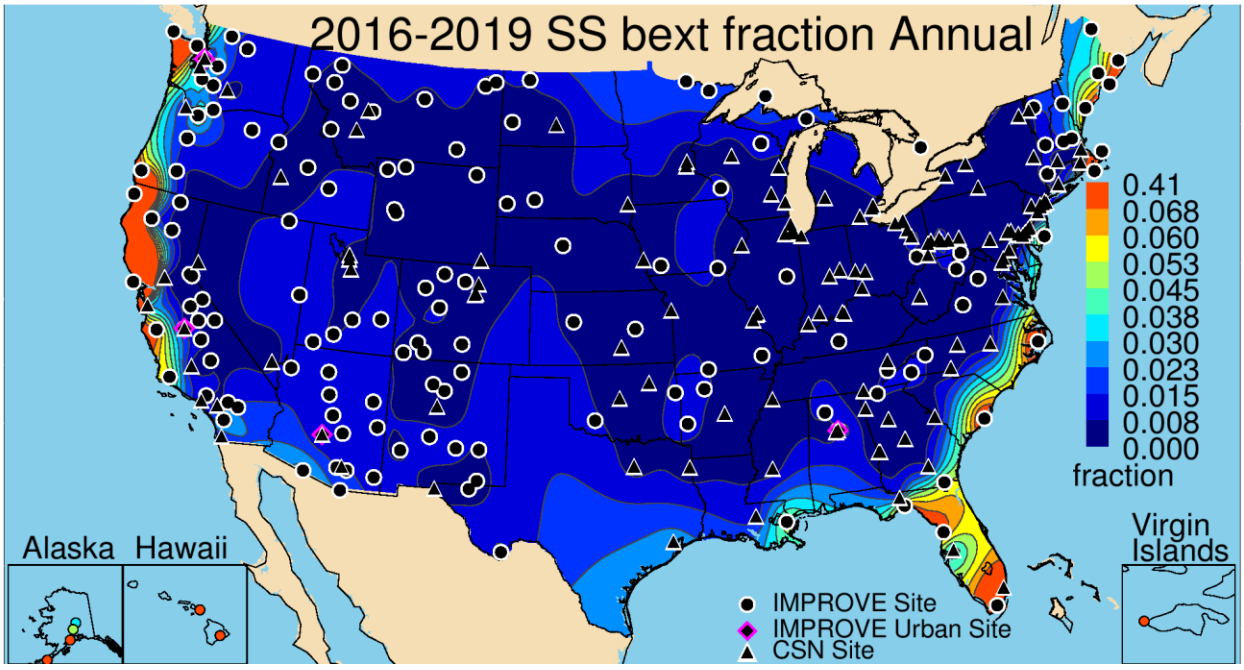

Figure 4.2.6d. IMPROVE and CSN 2016–2019 annual mean fraction contributions of sea salt light extinction coefficient (b_{ext_SS}) to reconstructed aerosol b_{ext}. Wavelength corresponds to 550 nm.

4.2.7 Coarse Mass Light Extinction Coefficients

The spatial patterns of IMPROVE annual mean CM concentrations and b_{ext_CM} were similar (Figure 4.2.7a) since CM is treated as nonhygroscopic in the extinction algorithm. The highest b_{ext_CM} occurred at sites in southern New Mexico and stretched across the southern Great Plains into the central United States. Sites in regions of southern Arizona, Southern California,

and California's Central Valley also had higher b_{ext_CM}. The maximum b_{ext_CM} occurred at Virgin Islands NP (7.87 Mm^{-1}, VIIS1), Salt Creek, New Mexico (7.20 Mm^{-1}, SACR1), and Columbia River Gorge, Washington (7.19 Mm^{-1}, CORI1). Lower annual mean b_{ext_CM} occurred at sites across the Intermountain West, along the Appalachian Mountains, and in regions of the Northeast and Northwest (< 2 Mm^{-1}). The lowest b_{ext_CM} occurred at Haleakala Crater NP, Hawaii (0.59 Mm^{-1}, HACR1), and Crater Lake NP, Oregon (0.63 Mm^{-1}, CRLA1).

The annual mean spatial pattern in urban b_{ext_CM} followed that of the IMPROVE spatial pattern (Figure 4.2.7b). Higher b_{ext_CM} occurred at sites across the central United States, southern New Mexico and Arizona, Southern California, and the Central Valley of California. Additional hot spots of b_{ext_CM} occurred at sites in the Colorado Front Range, Salt Lake City, Utah, and Indianapolis, Indiana. The highest b_{ext_CM} occurred in Rubidoux, California (13.15 Mm^{-1}, 060658001). The lowest annual mean b_{ext_CM} occurred in the Intermountain West, northwestern and northeastern United States, and many sites in the eastern United States (<2 Mm^{-1}). Somewhat elevated levels of b_{ext_CM} (~4 Mm^{-1}) occurred at sites in the southeastern United States. The minimum annual mean b_{ext_CM} occurred Sieben Flats, Montana, near Helena (1.04 Mm^{-1}, 300490004).

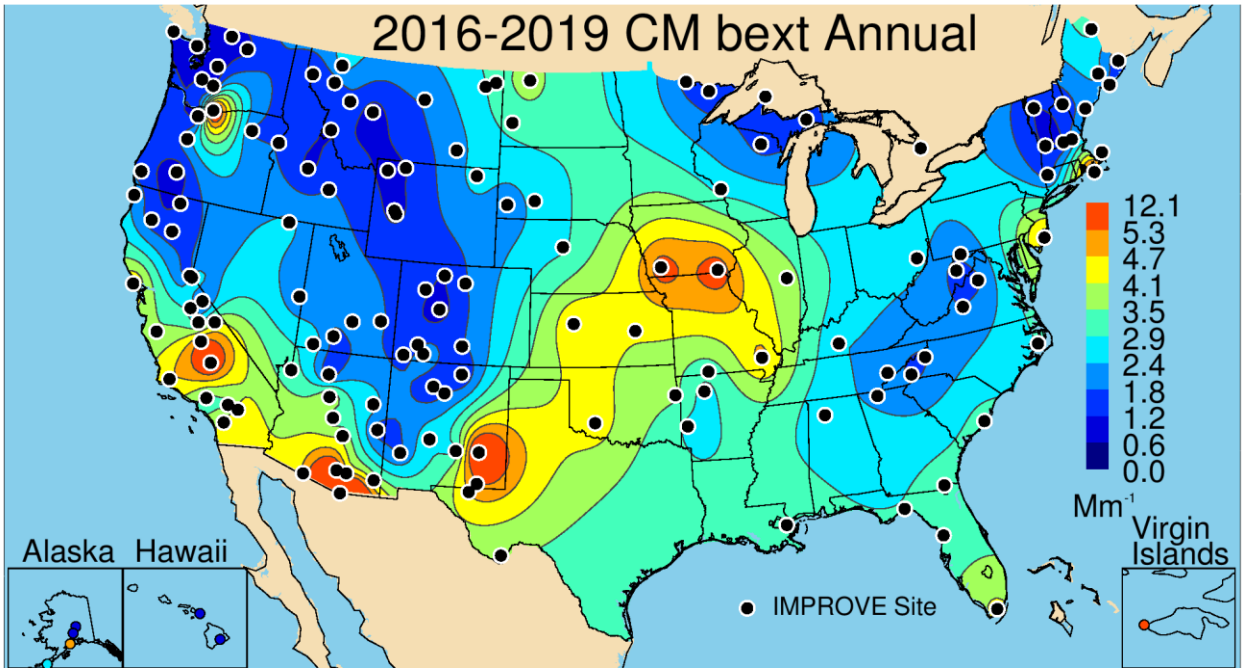

Figure 4.2.7a. IMPROVE 2016–2019 $PM_{2.5}$ reconstructed ambient annual mean light extinction coefficients for coarse mass (b_{ext_CM}, Mm^{-1}). Wavelength corresponds to 550 nm.

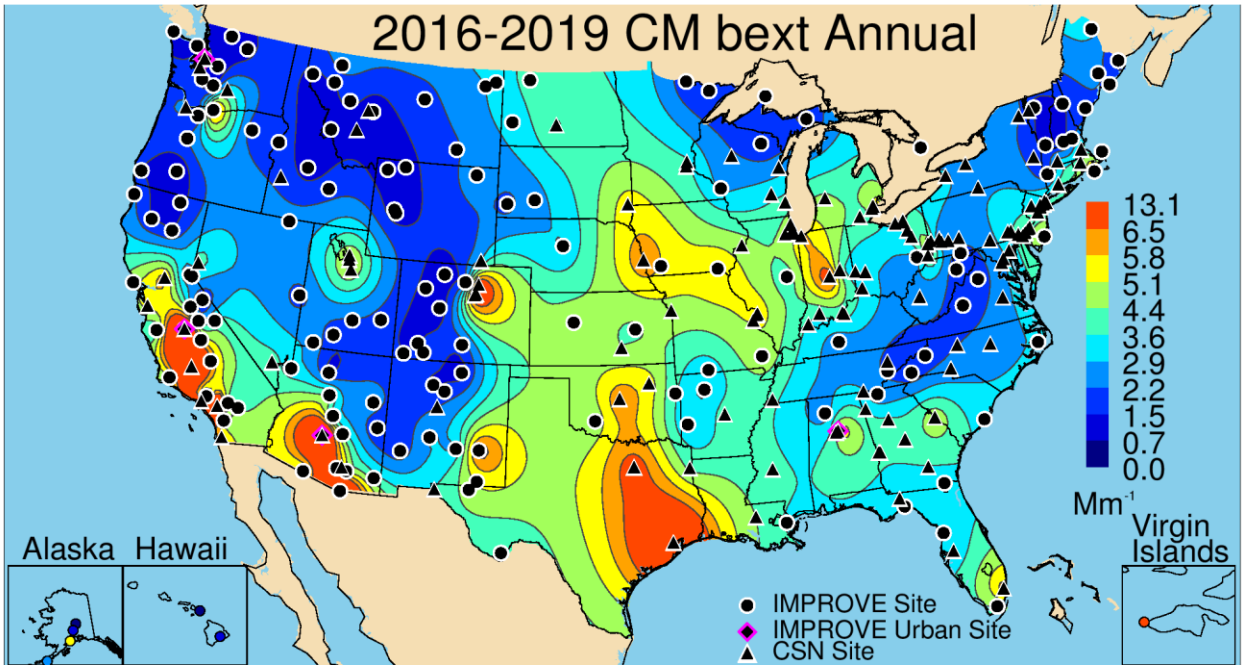

Figure 4.2.7b. IMPROVE and CSN 2016–2019 $PM_{2.5}$ reconstructed ambient annual mean light extinction coefficients for coarse mass (b_{ext_CM}, Mm^{-1}). Wavelength corresponds to 550 nm.

The annual mean IMPROVE fractional contributions of b_{ext_CM} to b_{ext_aer} ranged from 0.03 at Crater Lake NP, Oregon (CRLA1), to 0.32 in Saguaro West NP, Arizona (SAWE1) (see Figure 4.2.7c). The contributions of b_{ext_CM} to b_{ext_aer} were most important at sites in the southwestern United States, where b_{ext_CM} fractional contributions were ~0.25 or greater. Elevated fractions (0.10–0.15) occurred at sites across the western United States, reaching into the northern Great Plains. Fractional contributions at sites in the central United States were lower (<0.10) due to the importance of b_{ext_AN} contributions to b_{ext_aer}. Sites in the eastern United States and the northwestern United States had annual mean contributions of 0.10 or less.

The addition of annual mean b_{ext_CM} fractional contributions to b_{ext_aer} at sites with interpolated CM did not alter the spatial patterns seen for IMPROVE sites (Figure 4.2.7d). Contributions were highest at sites in the southwestern United States. Some urban hot spots occurred, such as increased contributions in the Front Range of Colorado (~0.19) and southern Florida (~0.15). Most of the eastern United States, especially sites in the Ohio River valley and Mid-Atlantic region had sites with low contributions (0.05 or less). Annual mean contributions ranged from 0.03 in Liberty, Pennsylvania (420030064), to 0.25 in Phoenix, Arizona (040139997).

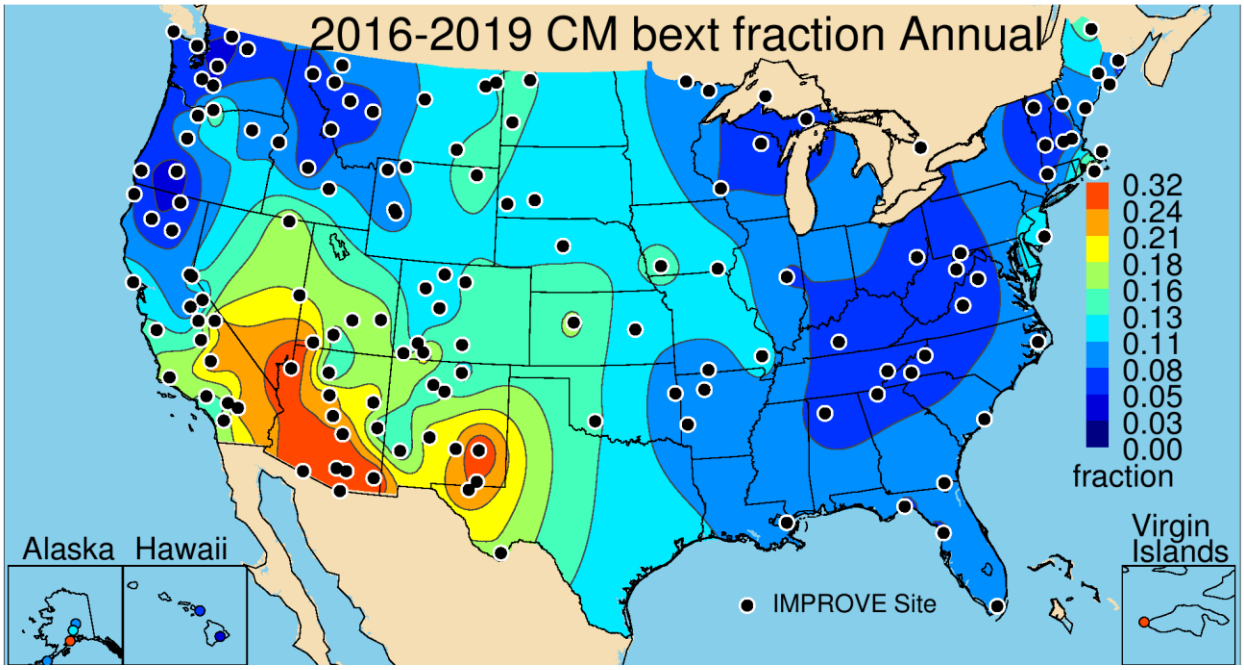

Figure 4.2.7c. IMPROVE 2016–2019 annual mean fraction contributions of coarse mass light extinction coefficient (b_{ext_CM}) to reconstructed aerosol b_{ext}. Wavelength corresponds to 550 nm.

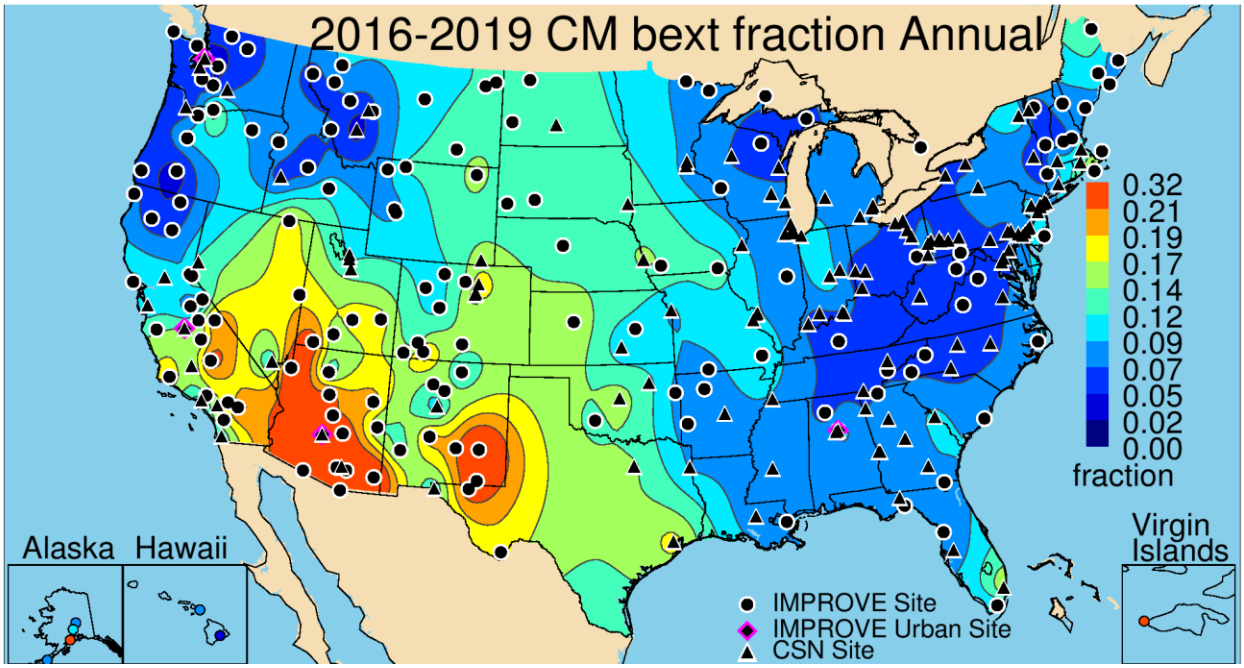

Figure 4.2.7d. IMPROVE and CSN 2016–2019 annual mean fraction contributions of coarse mass light extinction coefficient (b_{ext_CM}) to reconstructed aerosol b_{ext}. Wavelength corresponds to 550 nm.

4.2.8 Reconstructed Aerosol Light Extinction Coefficients

The 2016–2019 IMPROVE annual mean b_{ext_aer} is presented in Figure 4.2.8a. The east–west gradient observed for several species (especially b_{ext_AS}) was preserved in the aggregation of b_{ext_aer}, but sites with the highest b_{ext_aer} were in the central United States due to agricultural activity and in Florida due to biomass smoke impacts. Sites with the lowest b_{ext_aer} occurred in

the southwestern United States and the Intermountain West. Higher b_{ext_aer} occurred at sites in California and the northwestern United States. Annual mean b_{ext_aer} ranged from 7.48 Mm^{-1} in Haleakala Crater NP, Hawaii (HACR1), and 7.66 Mm^{-1} in White River NF, Colorado (WHRI1), to 50.65 Mm^{-1} in Bondville, Illinois (BOND1). Recall that the highest b_{ext_AN} fractional contribution to b_{ext_aer} (0.38) occurred at Bondville, Illinois (BOND1).

The addition of CSN sites preserved the large-scale gradients observed with IMPROVE sites, with higher b_{ext_aer} in the central and eastern United States compared to lower estimates at sites in the Intermountain West and southwestern United States (Figure 4.2.8b). The addition of sites in the eastern United States provided further spatial resolution that focused the area of high b_{ext_aer} (>50 Mm^{-1}) in the central United States, especially Indiana and Pennsylvania. High b_{ext_aer} also occurred at sites in Texas and at Gulf sites (>50 Mm^{-1}) and along the Central Valley of California. In fact, the highest annual mean b_{ext_aer} occurred at Bakersfield, California (88.71 Mm^{-1}, 0602090014). The maximum annual mean b_{ext_AN} also occurred at Bakersfield. The lowest annual mean b_{ext_aer} occurred in Cheyenne, Wyoming (18.49 Mm^{-1}, 560210100).

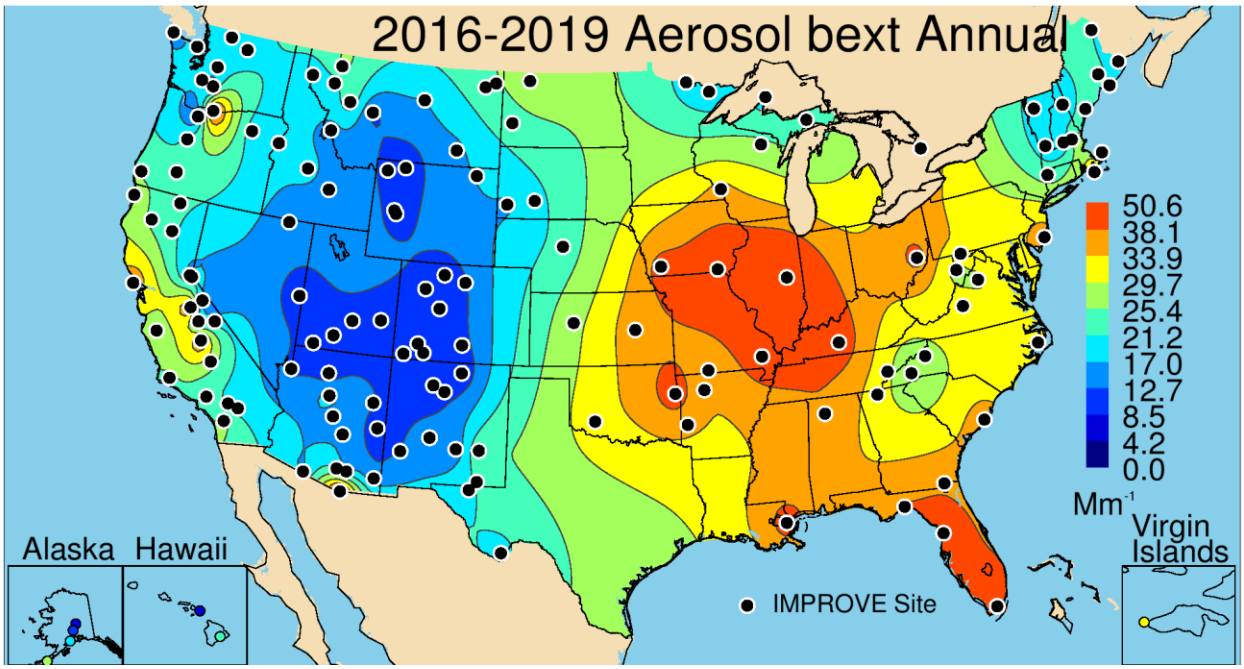

Figure 4.2.8a. IMPROVE 2016–2019 reconstructed ambient annual mean aerosol light extinction coefficients (b_{ext_aer}, Mm^{-1}) (no Rayleigh scattering). Wavelength corresponds to 550 nm.

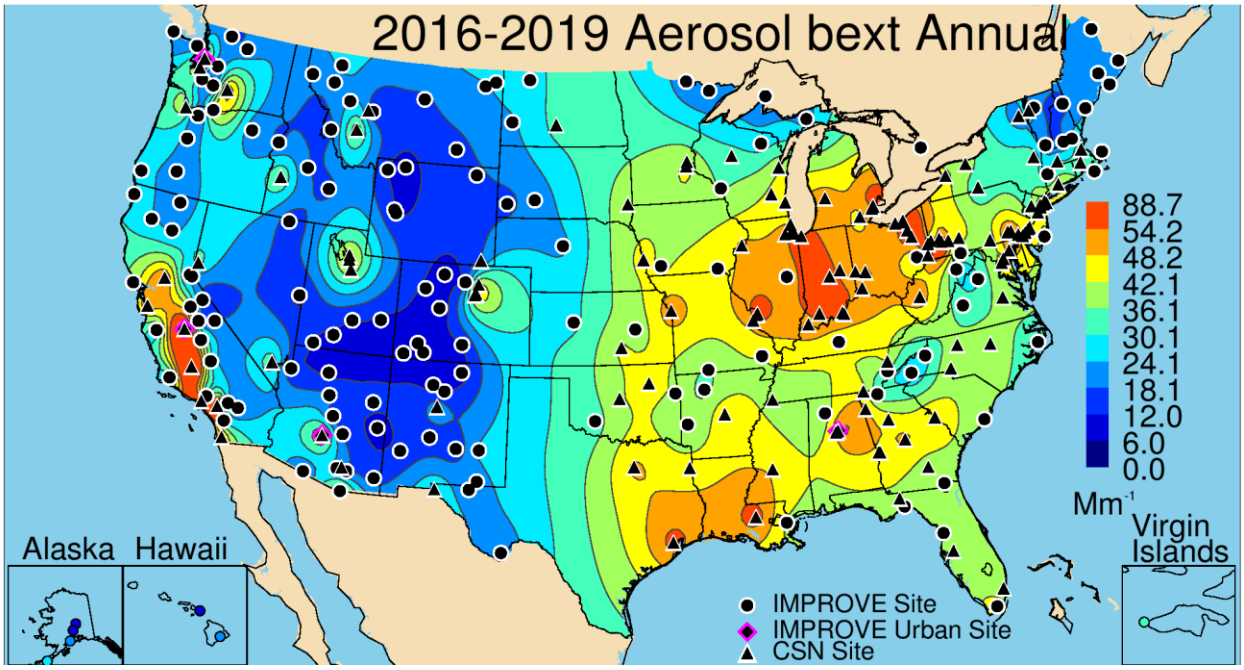

Figure 4.2.8b. IMPROVE and CSN 2016–2019 $PM_{2.5}$ reconstructed ambient annual mean aerosol light extinction coefficients (b_{ext_aer}, Mm^{-1}) (no Rayleigh scattering). Wavelength corresponds to 550 nm.

4.2.9 Reconstructed Total Light Extinction Coefficients

The spatial patterns in b_{ext_tot} are similar to b_{ext_aer} but increased by ~8–12 Mm^{-1} to account for site-specific Rayleigh scattering. IMPROVE annual mean b_{ext_tot} ranged from 15.67 Mm^{-1} at White River NF, Colorado (WHRI1), to 61.65 Mm^{-1} at Bondville, Illinois (BOND1) (see Figure 4.2.9a). Annual mean b_{ext_tot} at CSN sites (Figure 4.2.9b) ranged from 27.49 Mm^{-1} at Cheyenne, Wyoming (560210100), to 99.71 Mm^{-1} at Bakersfield, California (060290014).

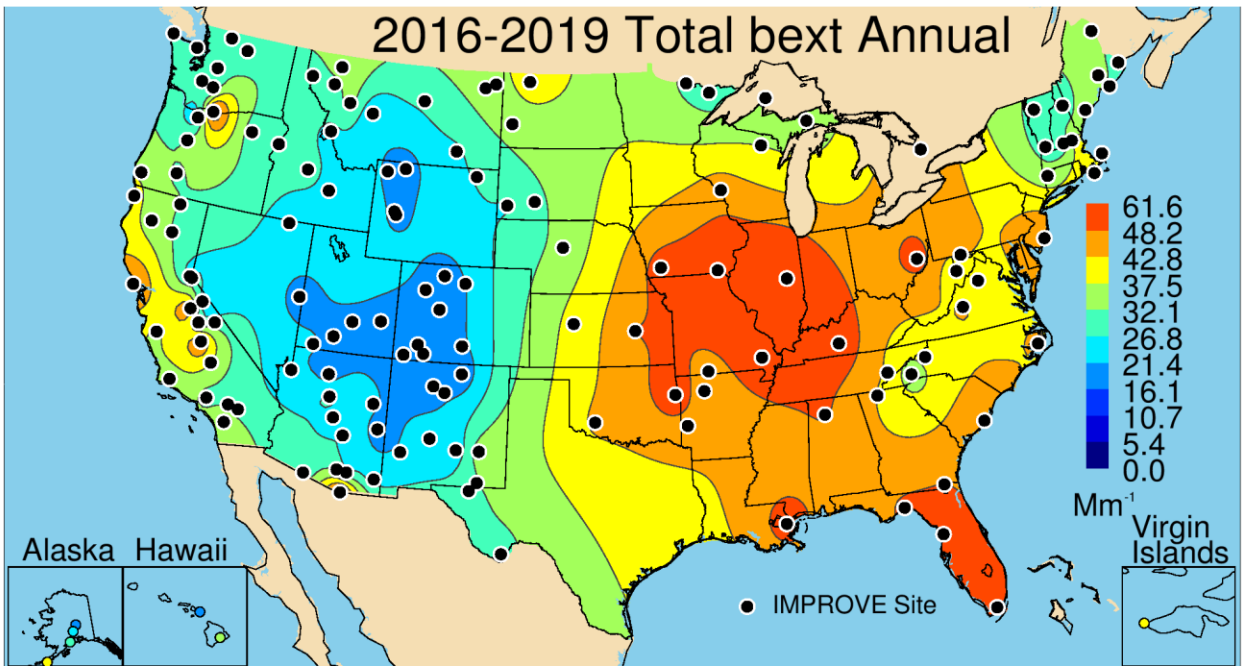

Figure 4.2.9a. IMPROVE 2016–2019 annual mean reconstructed ambient total light extinction coefficients (b_{ext_tot}, Mm^{-1}) (aerosol + Rayleigh). Wavelength corresponds to 550 nm.

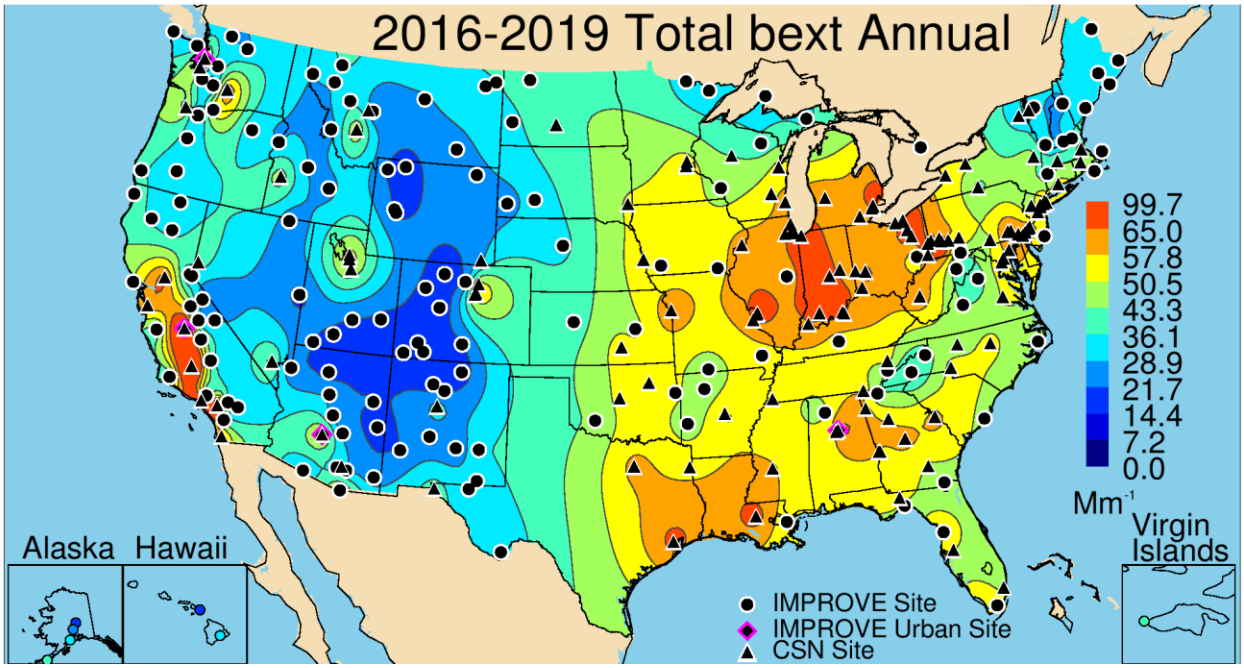

Figure 4.2.9b. IMPROVE 2016–2019 annual mean reconstructed ambient total light extinction coefficients (b_{ext_tot}, Mm^{-1}) (aerosol + Rayleigh). Wavelength corresponds to 550 nm.

4.2.10 Deciview

The 2016–2019 IMPROVE annual mean dv spatial pattern was very similar to the b_{ext_tot} pattern, as expected (see Figure 4.2.10a). Higher dv values (>15 dv) were observed at sites in the eastern United States, with the exception of northeastern sites (10–11 dv) . Lower values were observed at sites in the Intermountain West, especially at sites in the central Rocky Mountains of Colorado and northern New Mexico. Higher estimates were observed at sites in California (~15). Values at rural sites ranged from 4.49 dv at White River NF, Colorado (WHRI1), to 18.19 dv at Bondville, Illinois (BOND1).

Similar to the map of b_{ext_tot}, the addition of urban sites to the dv map in Figure 4.2.10b provided additional spatial resolution but did not change the overall patterns. The highest annual mean dv occurred at sites in the central United States and the Gulf area, as well as at sites in the Central Valley of California. Additional hot spots included sites in the Front Range of Colorado; Salt Lake City, Utah; Phoenix, Arizona; and Las Vegas, Nevada. Estimates ranged from 10.11 dv at Cheyenne, Wyoming (560210100), to 23.0 dv at Bakersfield, California (060290014).

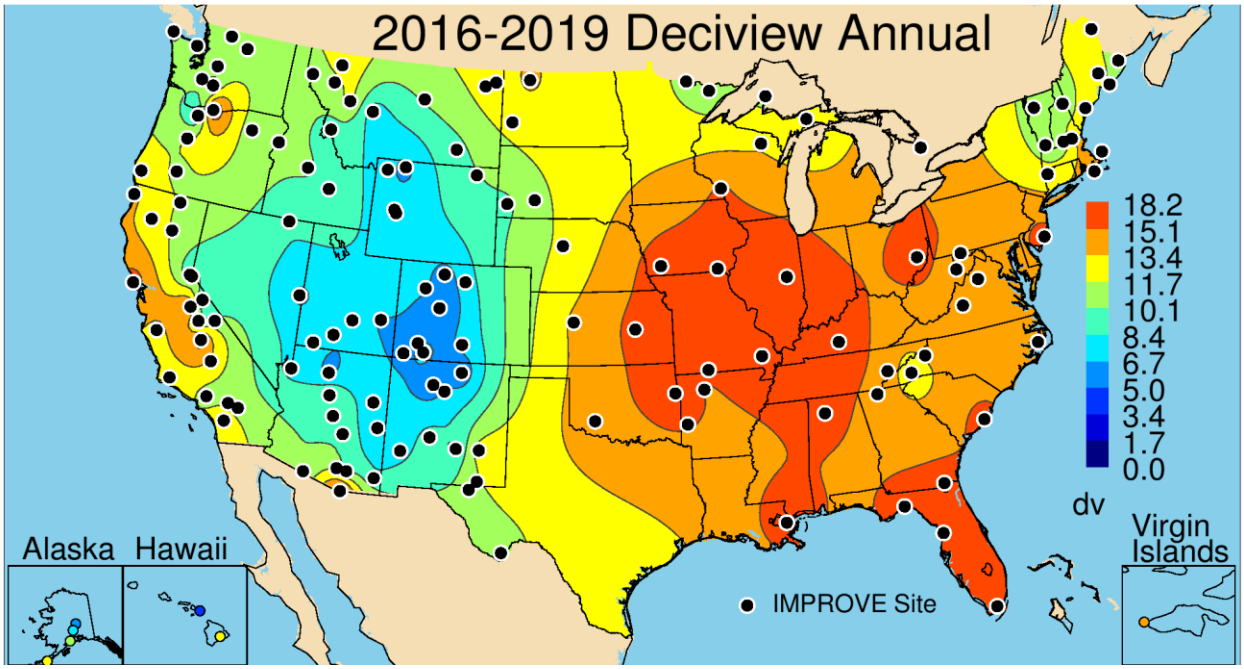

Figure 4.2.10a. IMPROVE 2016–2019 annual mean deciview (dv). Wavelength corresponds to 550 nm.

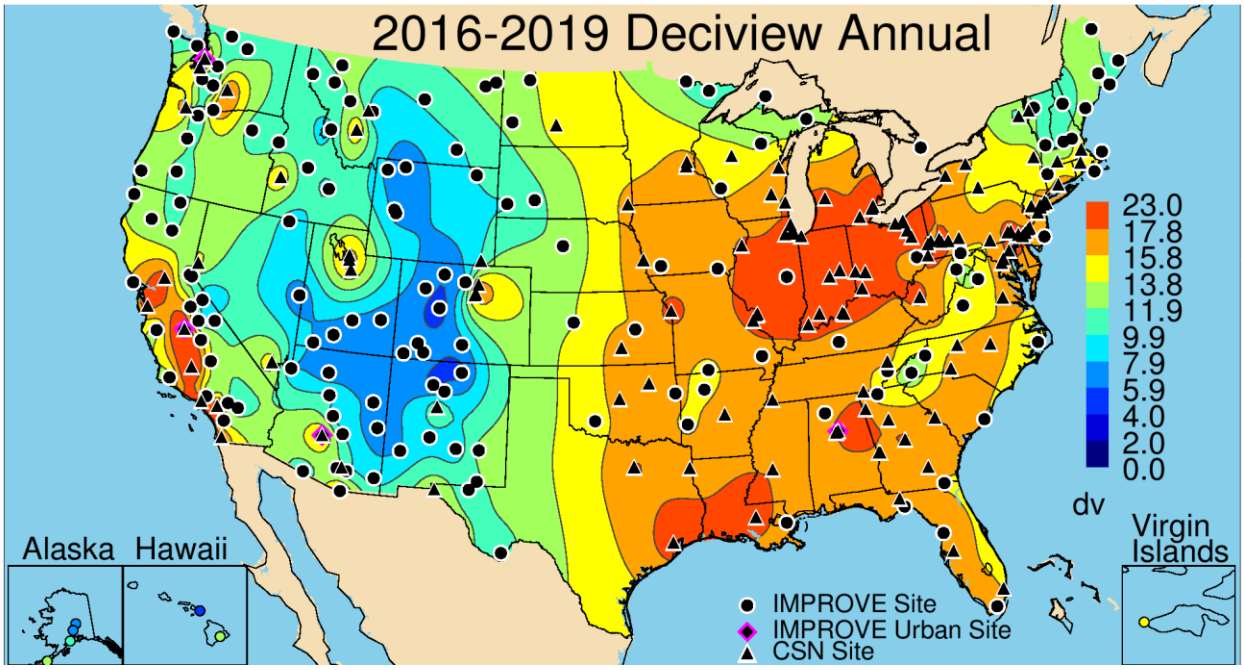

Figure 4.2.10b. IMPROVE and CSN 2016–2019 annual mean deciview (dv). Wavelength corresponds to 550 nm.

4.2.11 Summary

The spatial variability of speciated and total b_{ext_tot} depends on sources, transport, and environmental conditions, such as the impacts of RH on hygroscopic growth. While spatial patterns of speciated b_{ext} reflected the spatial patterns in mass presented in Chapter 2, they differed in some cases due to the uptake of water from species considered hygroscopic in the

reconstruction algorithm (i.e., AS, AN, and SS). For similar reasons, the spatial variability in fractional contributions of b_{ext} differed from species' fractional contributions to mass, depending on the roles of other species, some of which may be hygroscopic. In addition, the degree of light scattering efficiency of a particular species (e.g., mass scattering efficiency) will also influence the level of contribution of that species to b_{ext_tot}.

The highest annual mean b_{ext_AS} occurred at urban and rural sites in the eastern United States, where sources of SO_2 emissions are greatest, and high RH in summer can facilitate hygroscopic growth. Somewhat lower values occurred at sites in Virginia, West Virginia, and in the Northeast. A strong spatial gradient occurred along the central United States, resulting in relatively low b_{ext_AS} at sites across the West, due to lower emissions. Contributions of b_{ext_AS} to b_{ext_aer} were also highest in the East, typically greater than 0.3, and highest at rural sites. With the exception of sites in Hawaii, the annual mean fractional contribution of b_{ext_AS} to b_{ext_aer} did not exceed 0.5 at any rural or urban site. Fractional contributions also decreased at sites toward the West. Sites in the central United States had contributions around 0.25–0.3, and the lowest contributions occurred at sites in Idaho, Montana, and northern California (<0.15), likely due to the role of b_{ext_POM}.

Biomass smoke impacts at sites in the northwestern United States and Florida strongly influenced the b_{ext_POM} spatial pattern at rural sites, where the highest estimates of annual mean rural b_{ext_POM} occurred. Estimates were somewhat higher at sites in the southeastern United States, but still lower than at smoke-influenced sites. The lowest b_{ext_POM} at rural sites occurred in the southwestern United States. The annual mean b_{ext_POM} was higher in many urban areas, such as sites in the southeastern United States and the Central Valley of California, suggesting additional urban sources of POM. The contribution of b_{ext_POM} to b_{ext_aer} was highest at sites in the northwestern United States (>0.50), especially where contributions of b_{ext_AS} were low. Contributions of b_{ext_POM} at sites in the eastern United States were similar in magnitude or greater than contributions of b_{ext_AS}. At some urban sites in the western United States, contributions of b_{ext_POM} were lower than surrounding rural areas (e.g., the Central Valley of California and Salt Lake City, Utah) because of the role of b_{ext_AN}.

The highest annual mean b_{ext_AN} occurred at both urban and rural sites around the central United States due to agricultural activity in the region. Other hot spots occurred at urban sites in the West, such as Salt Lake City, Utah, and the Central Valley of California, suggesting additional urban and agricultural sources. Except for these areas, annual mean b_{ext_AN} was low across the United States. The fraction of b_{ext_aer} due to b_{ext_AN} was also highest at sites in the central United States, exceeding 0.3 across the region. Higher contributions were also observed at sites with hot spots of b_{ext_AN}.

Differences in urban and rural b_{ext} were most obvious for b_{ext_EC} compared to other species. Annual mean b_{ext_EC} at rural sites was high at some smoke-influenced sites in the northwestern United States and in Florida. However, at many rural sites in the eastern United States, annual mean b_{ext_EC} exceeded levels observed in the western United States. The lowest rural b_{ext_EC} occurred at sites across the Intermountain West. Urban annual mean b_{ext_EC} was much higher and more localized, with several hot spots in the West, such as Phoenix, Arizona, Las Vegas, Nevada, and urban sites in the Central Valley of California. Both regional and local

impacts of b_{ext_EC} occurred at sites in the East, such as hot spots in Georgia and Alabama, suggesting additional urban sources relative to surrounding rural areas.

Compared to other species, FD and CM have lower mass scattering efficiencies, which will reduce their influence on b_{ext_tot} on a per mass basis. Similar spatial patterns in b_{ext_FD} and b_{ext_CM} were observed at sites in the Central Valley of California and at sites in the southwestern United States, where estimates were the highest, suggesting similar sources. However, unlike b_{ext_FD}, annual mean b_{ext_CM} was elevated at sites in the central United States, corresponding to areas of agricultural activity. Both b_{ext_FD} and b_{ext_CM} were elevated at sites in the southeastern United States and the Virgin Islands site (VIIS1), consistent with the influence of transport of dust from North Africa. The contributions of b_{ext_FD} and b_{ext_CM} to b_{ext_aer} were highest at sites in the southwestern United States, around ~0.05–0.15 and 0.2–0.3, respectively.

Annual mean b_{ext_SS} was elevated at sites along the eastern and western coasts of the United States, near sources and in some regions where hygroscopic impacts were likely higher. Impacts from b_{ext_SS} farther inland were low, likely due to chloride loss from the filters. Sites in the Virgin Islands, Hawaii, and Alaska also had higher annual mean b_{ext_SS}. At many of these sites the contributions of b_{ext_SS} to b_{ext_aer} were larger than 0.1.

The spatial patterns in b_{ext_tot} and dv were similar and reflected the combined impacts from the species discussed above. Notably, the highest b_{ext_tot} and dv occurred at sites in the central United States and the Central Valley of California. Both regions corresponded to sites with the highest b_{ext_AN}, suggesting the importance of agricultural activity on visibility in these regions. Lower b_{ext_tot} and dv occurred at sites along the Appalachian Mountains, the Northeast, and especially the Intermountain West. While the role of biomass smoke is important to b_{ext_tot}, with elevated levels at sites in the Northwest and Florida, the role of agriculture appeared to dominate. The role of b_{ext_AS} on b_{ext_tot} was relatively low across the United States.

Tables of the 2016–2019 annual mean b_{ext} and b_{ext} fractions are reported for each site in Appendix 4.3 (IMPROVE and CSN b_{ext}) and 4.4 (IMPROVE and CSN b_{ext} fraction).

REFERENCES

EPA, U. S. (2001), U.S. Environmental Protection Agency, Interpolating relative humidity weighting factors to calculate visibility impairment and the effects of IMPROVE monitor outliers, *68-D-98-113, WA No. 3-39*, http://vista.cira.colostate.edu/Improve/wp-content/uploads/2016/03/DraftReportSept20.pdf.

EPA, U. S. (2003), U.S. Environmental Protection Agency, Guidance for tracking progress under the Regional Haze Rule, *EPA-454/B-03-004*, https://www.epa.gov/sites/default/files/2021-03/documents/tracking.pdf.

Hand, J. L., and Malm, W. C. (2006), Review of the IMPROVE equation for estimating ambient light extinction coefficients, Colorado State University, Fort Collins, CO, ISSN 0737-5352-71.

Hand, J. L., and Malm, W. (2007), Review of aerosol mass scattering efficiencies from ground-based measurements since 1990, *Journal of Geophysical Research: Atmospheres*, *112*(D16), 203, doi:10.1029/2007JD008484.

Hand, J. L., Prenni, A. J., Schichtel, B. A., Malm, W. C., and Chow, J. C. (2019), Trends in remote PM2.5 residual mass across the United States: Implications for aerosol mass reconstruction in the IMPROVE network, *Atmospheric Environment*, *203*, 141-152, doi:10.1016/j.atmosenv.2019.01.049.

Lowenthal, D. H., and Kumar, N. (2003), PM2.5 mass and light extinction reconstruction in IMPROVE, *Journal of the Air & Waste Management Association*, *53*(9), 1109-1120, https://doi.org/10.1080/10473289.2003.10466264.

Malm, W. C., Sisler, J. F., Huffman, D., Eldred, R. A., and Cahill, T. A. (1994), Spatial and seasonal trends in particle concentration and optical extinction in the United States, *Journal of Geophysical Research: Atmospheres*, *99*(D1), 1347-1370, https://doi.org/10.1029/93JD02916.

Malm, W. C., and Kreidenweis, S. M. (1997), The effects of models of aerosol hygroscopicity on the apportionment of extinction, *Atmospheric Environment*, *31*(13), 1965-1976, https://doi.org/10.1016/S1352-2310(96)00355-X.

Malm, W. C., Day, D. E., Carrico, C., Kreidenweis, S. M., Collett Jr, J. L., McMeeking, G., Lee, T., Carrillo, J., and Schichtel, B. (2005), Intercomparison and closure calculations using measurements of aerosol species and optical properties during the Yosemite Aerosol Characterization Study, *Journal of Geophysical Research: Atmospheres*, *110*(D14), D14302, doi:10.1029/2004JD005494.

Malm, W. C., and Hand, J. L. (2007), An examination of the physical and optical properties of aerosols collected in the IMPROVE program, *Atmospheric Environment*, *41*(16), 3407-3427, doi:10.1016/j.atmosenv.2006.12.012.

Pitchford, M. L., and Malm, W. C. (1994), Development and applications of a standard visual index, *Atmospheric Environment*, *28*(5), 1049-1054, https://doi.org/10.1016/1352-2310(94)90264-X.

Pitchford, M., Malm, W. C., Schichtel, B. A., Kumar, N., Lowenthal, D., and Hand, J. L. (2007), Revised algorithm for estimating light extinction from IMPROVE particle speciation data, *Journal of the Air & Waste Management Association*, *57*(11), 1326-1336, doi:10.3155/1047-3289.57.11.1326.

Prenni, A., Hand, J., Malm, W., Copeland, S., Luo, G., Yu, F., Taylor, N., Russell, L., and Schichtel, B. (2019), An examination of the algorithm for estimating light extinction from IMPROVE particle speciation data, *Atmospheric Environment*, *214*, 116880, https://doi.org/10.1016/j.atmosenv.2019.116880.